

# Cluster-Based Generalized Additive Models Informed by Random Fourier Features

Xin Huang<sup>a,\*</sup>, Jia Li<sup>b</sup>, Jun Yu<sup>a</sup>

<sup>a</sup>*Department of Mathematics and Mathematical Statistics, Umeå University, Umeå, 901 87, Sweden*

<sup>b</sup>*Department of Statistics, The Pennsylvania State University, University Park, 16802, PA, USA*

---

## Abstract

In the development of learning systems, there is an ongoing need to reconcile the strong predictive performance offered by opaque black-box models with the level of transparency required for critical applications. This work introduces a methodological framework that combines spectral representation learning with transparent statistical modeling to construct a mixture of generalized additive models (GAMs). The approach utilizes random Fourier feature embeddings to uncover locally adaptive structures within the data. High-dimensional random feature representations are compressed via principal component analysis to derive a latent space that informs a Gaussian mixture model, which performs soft clustering to partition the input space into distinct regimes. Within each cluster, a local GAM captures nonlinear univariate effects through interpretable spline-based smoothers. Numerical experiments across diverse regression benchmarks demonstrate that the proposed method consistently improves upon classical global interpretable models by effectively modeling data heterogeneity. Furthermore, the mixture-of-GAMs framework achieves performance comparable to explainable boosting machine, random forest, and multilayer perceptron on certain tasks. Overall, this construction provides a principled approach for integrating representation learning with transparent statistical modeling.

*Keywords:* Generalized additive models; Random Fourier features; Gaussian mixture models; Latent representation learning; Interpretable adaptive regression

---

## 1. Introduction

Suppose that we are given a dataset  $\{(\mathbf{x}_i, y_i)\}_{i=1}^N$  consisting of  $N$  independent observations from a joint distribution of random variables  $(X, Y)$ , where  $X \in \mathbb{R}^p$  denotes the predictor variable and  $Y \in \mathbb{R}$  is the corresponding response variable. In a regression setting, the objective is to estimate the target function

$$m(\mathbf{x}) = \mathbb{E}[Y|X = \mathbf{x}] \quad (1)$$

which is the conditional expectation of the response given the predictor vector  $\mathbf{x}$ , based on the available training data.

---

\*Corresponding author.

Email addresses: [xin.huang@umu.se](mailto:xin.huang@umu.se) (Xin Huang), [jol2@psu.edu](mailto:jol2@psu.edu) (Jia Li), [jun.yu@umu.se](mailto:jun.yu@umu.se) (Jun Yu)

A recent line of work strives to reconcile the strong predictive performance of opaque machine-learning methods with the transparency offered by statistical modeling. Notably, the *mixture of linear models* (MLM) framework introduced in [38] constructs mixture models whose components are trained with guidance from predictive models learned by a *deep neural network* (DNN). This training mechanism is referred to as co-supervision. In this method, the predictive model with  $L$  mixture components is expressed as

$$\begin{aligned}\hat{m}(\mathbf{x}) &= \sum_{\ell=1}^L \gamma_\ell(\mathbf{x}) r_\ell(\mathbf{x}), \\ r_\ell(\mathbf{x}) &= \alpha_\ell + \mathbf{x}^\top \boldsymbol{\beta}_\ell, \quad \ell = 1, \dots, L,\end{aligned}\tag{2}$$

where  $r_\ell(\mathbf{x})$  denotes the linear regression model associated with cluster  $\ell$ , and the mixture weights  $\gamma_\ell(\mathbf{x})$  are the posterior probabilities of cluster  $\ell$  given  $\mathbf{x}$ , both estimated under the co-supervision of a DNN. Specifically, the intermediate representations extracted from the hidden layers of a DNN are grouped to generate cluster labels for the input points. Then a *Gaussian Mixture Model* (GMM) is fitted on the input  $\mathbf{x}$  for each cluster. Let the estimated density of the GMM for cluster  $\ell$  be  $v_\ell(\mathbf{x})$  and the corresponding prior be  $\pi_\ell$ , the mixture weights are given by

$$\gamma_\ell(\mathbf{x}) = \frac{\pi_\ell v_\ell(\mathbf{x})}{\sum_{\ell'=1}^L \pi_{\ell'} v_{\ell'}(\mathbf{x})}, \quad \ell = 1, \dots, L.$$

The MLM framework compromises between accuracy and interpretability: the DNN provides a high-quality surrogate of the regression function, while the mixture of linear models yields local interpretability. Moreover, the tradeoff between accuracy and interpretability is controlled by the number of mixture components.

Despite the insights provided by MLMs via co-supervision with DNNs, several practical considerations motivate the exploration of alternative formulations. While the use of local linear models ensures interpretability, it can be restrictive when the underlying regression surface exhibits smooth nonlinear structure or heterogeneous marginal effects. Introducing nonlinearity under appropriate structural constraints may substantially improve predictive accuracy while retaining a sufficient degree of interpretability. Moreover, the clustering mechanism in the MLM framework of [38] depends critically on the architecture of the supervising DNN, raising the question of how effective clustering can be achieved using alternative, potentially more explainable representation models. In this work, we address both limitations.

### 1.1. Overview of the Proposed Approach

Motivated by the objective of establishing a more flexible and structurally interpretable alternative to DNN co-supervised MLMs, we introduce a mixture framework informed by *random Fourier feature* (RFF) embeddings. Random Fourier features are widely applied as scalable, latent-feature-based representations that provide kernel-level expressivity while remaining computational tractability. Moreover, they have demonstrated robust empirical performance alongside rigorous theoretical foundations in large-scale learning applications [1, 29]. Specifically, the RFF approximation of the target regression function  $m(\mathbf{x})$  in (1) is defined as

$$\bar{m}(\mathbf{x}) = \sum_{k=1}^K \beta_k e^{i\omega_k \cdot \mathbf{x}},$$

where the frequencies  $\omega_k \in \mathbb{R}^p$  are sampled independently and identically for  $k = 1, \dots, K$  from a spectral density  $\rho(\omega) : \mathbb{R}^p \rightarrow \mathbb{R}^+$  that encodes prior smoothness assumptions on the target function. This construction reconciles representation learning with statistical modeling by inducing a linear model in a randomized feature space, supported by principled approximation and generalization guarantees [2, 34].

To exploit the structural information learned by the RFF model, we develop a clustering strategy based on its spectral characteristics. In particular, we combine the learned amplitudes  $\{\beta_k\}_{k=1}^K$  with their corresponding frequencies  $\{\omega_k\}_{k=1}^K$  to construct a compact frequency-domain representation. Analogously to the MLM framework, a Gaussian mixture model is applied to a low-dimensional latent representation obtained via *principal component analysis* (PCA) of the amplitude-weighted Fourier features, yielding a soft partition of the data into  $L$  mixture components.

Given the trigonometric representation of the RFF model  $\bar{m}(\mathbf{x})$ , we train a local *generalized additive model* (GAM) within each cluster  $\ell = 1, \dots, L$ . The cluster-specific model is defined as

$$\tilde{f}^{(\ell)}(\mathbf{x}) = \alpha^{(\ell)} + \sum_{j=1}^p g_j^{(\ell)}(x_j), \quad \text{with} \quad g_j^{(\ell)}(x_j) = \sum_{q=1}^{Q_j} \theta_{j,q}^{(\ell)} \phi_{j,q}(x_j),$$

where  $\alpha^{(\ell)}$  denotes the intercept and  $g_j^{(\ell)} : \mathbb{R} \rightarrow \mathbb{R}$  represents the contribution of the  $j$ -th covariate  $x_j$  of the predictor vector  $\mathbf{x} = [x_1, \dots, x_p]^\top$  to the  $\ell$ -th local model. Each univariate function  $g_j^{(\ell)}$  is expressed as a linear combination of  $Q_j$  spline basis functions  $\{\phi_{j,q}(x_j)\}_{q=1}^{Q_j}$  with corresponding coefficients  $\theta_{j,q}^{(\ell)}$ . Finally, combining the cluster-specific GAMs  $\tilde{f}^{(\ell)}(\mathbf{x})$  with the soft assignment probabilities  $\gamma_\ell(\mathbf{x})$  obtained from the fitted Gaussian mixture model yields the overall mixture-of-GAMs regression:

$$\tilde{m}(\mathbf{x}) = \sum_{\ell=1}^L \gamma_\ell(\mathbf{x}) \tilde{f}^{(\ell)}(\mathbf{x}).$$

Unlike DNN-co-supervised MLMs, the proposed framework combines an RFF-based latent representation with cluster-specific GAMs to provide a locally adaptive regression model with intrinsically interpretable nonlinear responses. The resulting mixture model preserves expressivity while enabling transparent analysis of covariate effects within each cluster component.

## 1.2. Main Contributions

Building on the framework described above, the main contributions of this study are summarized as follows:

- (1) *A novel mixture-of-GAMs framework.* We propose a unified regression framework in which locally adaptive and intrinsically interpretable additive models are constructed using a latent representation learned by random Fourier features.
- (2) *RFF-based clustering of data.* We introduce an RFF-based frequency-domain representation to guide soft clustering of the data through a Gaussian mixture model, thereby inducing locally specialized predictive models for each mixture component.
- (3) *Improved local modeling via spline representations.* Extending mixture of linear models, the proposed method employs cluster-specific generalized additive models, enabling the capture of non-linear and interpretable covariate effects within each mixture component via spline-based fitting.

(4) *Extensive numerical validation.* We demonstrate that the proposed framework consistently improves predictive performance over global interpretable models and mixture-of-linear baselines across multiple real-world regression benchmarks.

### 1.3. Related Literature

Random Fourier features have been widely used to approximate kernel methods and to construct representations that capture geometric structure in data. Several recent works explore how such representations can support interpretability, clustering, or end-to-end kernel learning.

The G-NAMRFF model [32] integrates RFF-based kernel approximations into additive models for graph-structured learning tasks. Although aiming at interpretability, it focuses on graph prediction problems rather than tabular regression, and it employs a single global additive model rather than a mixture of cluster-specific models.

Random Fourier features have also been applied to scalable clustering. [10] show that  $k$ -means applied to RFF embeddings provides an efficient approximation to kernel  $k$ -means. Their work informs our use of Fourier representations to approximate kernel geometry, though their setting is for unsupervised clustering rather than regression with local interpretable models.

A more flexible clustering perspective appears in Clustering-Induced Kernel Learning (CIK, [24]), which jointly learns cluster assignments and kernel parameters using reparameterized RFFs within a Dirichlet-process mixture framework. Unlike CIK, which is primarily developed for classification and kernel learning, our method employs an unsupervised PCA-GMM clustering step on Fourier features and focuses on interpretability through cluster-specific GAMs.

End-to-end kernel learning with generative RFFs has been explored by [14], which optimizes the spectral distribution jointly with a classifier to improve robustness. This approach is likewise designed for classification rather than regression, and the Fourier features serve as learnable parameters rather than as a tool for revealing structure useful for interpretable mixture modeling.

Finally, mixture models informed by latent representations, such as the mixture-of-linear-models framework of [38] and related co-supervised architectures [37], demonstrate how geometric information extracted from a deep neural network can guide localized modeling. Our approach differs by avoiding deep-network co-supervision and by combining RFF-based unsupervised clustering with component-specific GAMs, enabling transparent visualization and interpretation of nonlinear covariate effects.

The remainder of this manuscript is organized as follows. Section 2 reviews the necessary preliminaries, including the random Fourier feature model and its connection to kernel regression, principal component analysis for feature extraction, Gaussian mixture models for soft clustering assignments, and generalized additive models used for interpretable local modeling. Section 3 presents the proposed methodology, detailing the construction of the latent Fourier representation, the clustering procedure, and the mixture-of-GAMs estimator. Section 4 reports numerical experiments, with case studies on the California Housing dataset, using both the full Fourier representation and interpretable spatial Fourier features, and on the Airfoil Self-Noise dataset, implementing additionally a perturbation-based data augmentation strategy. Section 5 concludes the findings and discusses potential directions for future research. For clarity and reference, the notation and abbreviations used in this work are summarized in Tables C.2 and C.1 of Appendix C.

## 2. Preliminaries

### 2.1. Random Fourier Feature Model and Kernel Regression

Given a dataset  $\{(\mathbf{x}_i, y_i)\}_{i=1}^N$ , where each sample of covariate vector  $\mathbf{x}_i \in \mathbb{R}^p$  with the corresponding response  $y_i \in \mathbb{R}$ , the kernel method approximates the target function  $m(\mathbf{x})$  given in (1) by

$$m_\kappa(\mathbf{x}) = \sum_{i=1}^N \eta_i \kappa(\mathbf{x}, \mathbf{x}_i), \quad (3)$$

where  $\kappa : \mathbb{R}^p \times \mathbb{R}^p \rightarrow \mathbb{R}$  is a symmetric, positive semidefinite kernel function. A commonly used kernel is the *Gaussian radial basis function* (RBF) kernel, defined by

$$\kappa(\mathbf{x}, \mathbf{x}') = \kappa_\sigma(\mathbf{x} - \mathbf{x}') = \exp\left(-\frac{\|\mathbf{x} - \mathbf{x}'\|^2}{2\sigma^2}\right), \quad (4)$$

where  $\sigma > 0$  is the bandwidth parameter. The coefficients  $\boldsymbol{\eta} = [\eta_1, \dots, \eta_N]^\top$  are obtained by minimizing the regularized empirical risk:

$$\min_{\boldsymbol{\eta} \in \mathbb{R}^N} \left\{ \sum_{i=1}^N \left( \sum_{j=1}^N \eta_j \kappa(\mathbf{x}_i, \mathbf{x}_j) - y_i \right)^2 + \lambda \boldsymbol{\eta}^\top \boldsymbol{\Xi} \boldsymbol{\eta} \right\},$$

where  $\lambda > 0$  is a Tikhonov regularization parameter and  $\boldsymbol{\Xi} \in \mathbb{R}^{N \times N}$  is the *kernel matrix* with entries

$$\boldsymbol{\Xi}_{i,j} = \kappa(\mathbf{x}_i, \mathbf{x}_j) \quad \text{for } i, j = 1, \dots, N.$$

The solution to this optimization problem is given by the *kernel ridge regression* equation:

$$(\boldsymbol{\Xi} + \lambda \mathbf{I}) \boldsymbol{\eta} = \mathbf{y}. \quad (5)$$

where  $\mathbf{y} = [y_1, \dots, y_N]^\top \in \mathbb{R}^N$  is the response data. For large-scale datasets, the computational cost for solving equation (5) using direct methods is  $\mathcal{O}(N^3)$ , which motivates the development of efficient kernel approximations such as random Fourier features.

For any continuous, symmetric, and positive semidefinite kernel function  $\kappa(\mathbf{x}, \mathbf{x}')$ , *Mercer's theorem* [3, 36] guarantees the existence of a feature map  $\phi : \mathbb{R}^p \rightarrow \mathcal{H}$ , where  $\mathcal{H}$  is a Hilbert space, such that:

$$\kappa(\mathbf{x}, \mathbf{x}') = \langle \phi(\mathbf{x}), \phi(\mathbf{x}') \rangle_{\mathcal{H}} \quad \text{for all } \mathbf{x}, \mathbf{x}' \in \mathbb{R}^p. \quad (6)$$

More specifically, consider the integral operator  $T_\kappa : L^2(\Omega) \rightarrow L^2(\Omega)$  defined on a compact domain  $\Omega \subset \mathbb{R}^p$  by

$$(T_\kappa f)(\mathbf{x}) := \int_{\Omega} \kappa(\mathbf{x}, \mathbf{x}') f(\mathbf{x}') d\mathbf{x}' \quad \text{for all } f \in L^2(\Omega).$$

Then there exists an orthonormal sequence of eigenfunctions  $\{\psi_k\}_{k=1}^\infty \subset L^2(\Omega)$ , with corresponding nonnegative eigenvalues  $\{\lambda_k\}_{k=1}^\infty$ , such that the kernel function admits the expansion

$$\kappa(\mathbf{x}, \mathbf{x}') = \sum_{k=1}^{\infty} \lambda_k \psi_k(\mathbf{x}) \psi_k(\mathbf{x}').$$

This representation induces a feature map

$$\phi(\mathbf{x}) := \left( \sqrt{\lambda_1} \psi_1(\mathbf{x}), \sqrt{\lambda_2} \psi_2(\mathbf{x}), \dots \right) \in \ell^2,$$

where  $\ell^2$  is the Hilbert space of square-summable sequences. With this embedding, the kernel function admits an inner product representation:

$$\kappa(\mathbf{x}, \mathbf{x}') = \langle \phi(\mathbf{x}), \phi(\mathbf{x}') \rangle_{\ell^2}.$$

The identity (6) allows us to interpret kernel methods as linear models in a (possibly infinite-dimensional) feature space. For example, the Gaussian RBF kernel  $\kappa_\sigma(\mathbf{x} - \mathbf{x}')$  in (4) corresponds to the inner product in an infinite-dimensional Hilbert space, even though its feature representation is not available in closed form.

Using the representation (6), the kernel regression function introduced in (3) can be expressed as

$$m_\kappa(\mathbf{x}) = \sum_{i=1}^N \eta_i \kappa(\mathbf{x}, \mathbf{x}_i) = \langle \phi(\mathbf{x}), \sum_{i=1}^N \eta_i \phi(\mathbf{x}_i) \rangle_{\mathcal{H}} =: \langle \phi(\mathbf{x}), \boldsymbol{\varphi} \rangle_{\mathcal{H}},$$

where we define the *representer*  $\boldsymbol{\varphi} := \sum_{i=1}^N \eta_i \phi(\mathbf{x}_i) \in \mathcal{H}$ . This formulation highlights how the prediction at a new covariate vector  $\mathbf{x}$  can be obtained via an inner product in the feature space, even though computations are performed in the input space through the kernel function.

Moreover, *Bochner's theorem* [3, 41] builds a connection between a properly scaled positive definite radial basis function  $\kappa : \mathbb{R}^p \rightarrow \mathbb{R}^+$  and a probability density  $\rho : \mathbb{R}^p \rightarrow \mathbb{R}^+$  through the Fourier transform over frequency domain parameter  $\boldsymbol{\omega} \in \mathbb{R}^p$ , allowing an expression using expectation over the distribution of frequency variable  $\boldsymbol{\omega}$  under probability density  $\rho$  by:

$$\kappa(\mathbf{x} - \mathbf{x}') = \int_{\mathbb{R}^p} \rho(\boldsymbol{\omega}) e^{i\boldsymbol{\omega} \cdot (\mathbf{x} - \mathbf{x}')} d\boldsymbol{\omega} = \mathbb{E}_{\rho(\boldsymbol{\omega})} [\zeta_{\boldsymbol{\omega}}(\mathbf{x}) \zeta_{\boldsymbol{\omega}}(\mathbf{x}')^*], \quad (7)$$

where  $\zeta_{\boldsymbol{\omega}}(\mathbf{x}) := e^{i\boldsymbol{\omega} \cdot \mathbf{x}}$  denotes the complex trigonometric feature function, and  $(\cdot)^*$  denotes complex conjugation. The expectation in (7) can be approximated under the Monte Carlo scheme:

$$\mathbb{E}_{\rho(\boldsymbol{\omega})} [\zeta_{\boldsymbol{\omega}}(\mathbf{x}')^* \zeta_{\boldsymbol{\omega}}(\mathbf{x})] \approx \frac{1}{K} \sum_{k=1}^K e^{i\boldsymbol{\omega}_k \cdot \mathbf{x}} e^{-i\boldsymbol{\omega}_k \cdot \mathbf{x}'} =: \varsigma(\mathbf{x})^\top \varsigma(\mathbf{x}')^*,$$

where the feature map  $\varsigma : \mathbb{R}^p \rightarrow \mathbb{C}^K$  is defined by

$$\varsigma(\mathbf{x}) := [e^{i\boldsymbol{\omega}_1 \cdot \mathbf{x}}, e^{i\boldsymbol{\omega}_2 \cdot \mathbf{x}}, \dots, e^{i\boldsymbol{\omega}_K \cdot \mathbf{x}}]^\top, \quad (8)$$

with independent identically distributed frequency samples  $\{\boldsymbol{\omega}_k\}_{k=1}^K$  drawn from  $\rho(\boldsymbol{\omega})$ . This yields the *random Fourier feature approximation* of positive definite kernel functions

$$\kappa(\mathbf{x} - \mathbf{x}') \simeq \varsigma(\mathbf{x})^\top \varsigma(\mathbf{x}')^*.$$

Substituting this approximation into the kernel regression model, we obtain

$$m_\kappa(\mathbf{x}) = \sum_{i=1}^N \eta_i \kappa(\mathbf{x} - \mathbf{x}_i) \simeq \sum_{i=1}^N \eta_i \varsigma(\mathbf{x})^\top \varsigma(\mathbf{x}_i)^* = \varsigma(\mathbf{x})^\top \left( \sum_{i=1}^N \eta_i \varsigma(\mathbf{x}_i)^* \right) =: \varsigma(\mathbf{x})^\top \boldsymbol{\beta},$$

where  $\beta := \sum_{i=1}^N \eta_i \varsigma(\mathbf{x}_i)^* \in \mathbb{C}^K$ . This defines the *random Fourier feature model*:

$$\bar{m}(\mathbf{x}) = \beta^\top \varsigma(\mathbf{x}) = \sum_{k=1}^K \beta_k e^{i\omega_k \cdot \mathbf{x}}, \quad (9)$$

which expresses the regression function as a linear combination of randomly sampled complex Fourier basis functions. By approximating shift-invariant kernels using trigonometric basis functions, this model provides a scalable and straightforward alternative to traditional kernel methods.

To estimate the coefficients  $\beta = [\beta_1, \dots, \beta_K]^\top \in \mathbb{C}^K$ , we solve a regularized least-squares problem using the available training data  $(\mathbf{x}_i, y_i)_{i=1}^N$ . Let  $\Phi \in \mathbb{C}^{N \times K}$  denote the design matrix with entries

$$\Phi_{ik} = e^{i\omega_k \cdot \mathbf{x}_i}, \quad \text{for } i = 1, \dots, N, \text{ and } k = 1, \dots, K,$$

and let  $\mathbf{y} = [y_1, \dots, y_N]^\top \in \mathbb{R}^N$  be the vector of observed responses. The coefficients  $\beta$  can then be obtained by minimizing the Tikhonov-regularized loss:

$$\min_{\beta \in \mathbb{C}^K} \{ \|\Phi\beta - \mathbf{y}\|_2^2 + \lambda \|\beta\|_2^2 \}, \quad (10)$$

where  $\lambda > 0$  is a regularization parameter controlling the smoothness of the fit. While we mainly focus on Tikhonov regularization in this work, alternative regularization schemes such as  $\ell_p$ -type penalties with  $p \leq 1$  can be considered to promote sparsity in the random feature coefficients and could be investigated in future work. The normal equations associated with the problem (10) are given by:

$$(\Phi^H \Phi + \lambda I_K) \beta = \Phi^H \mathbf{y}, \quad (11)$$

where  $\Phi^H$  denotes the Hermitian transpose of  $\Phi$ . This linear system can be efficiently solved using either direct solvers (e.g., Cholesky factorization) or iterative methods (e.g., conjugate gradient) for a moderate to large number of frequencies  $K$ . The inclusion of the  $\ell_2$  penalty term  $\lambda \|\beta\|_2^2$  helps mitigate overfitting and improves numerical stability, especially when the value of  $K$  is large or the input features are noisy.

Following the formulation in [12], a standard shallow neural network with one hidden layer takes the form

$$f(\mathbf{x}) = \sum_{k=1}^K a_k \sigma(w_k \cdot \mathbf{x} + c_k),$$

where  $\sigma(\cdot)$  denotes a nonlinear activation function,  $w_k \in \mathbb{R}^p$  are the hidden-layer weights,  $c_k \in \mathbb{R}$  are bias terms, and  $a_k \in \mathbb{R}$  are output-layer coefficients. From this perspective, the random Fourier feature model  $\bar{m}(\mathbf{x})$  in (9) can be understood as a neural network with one hidden layer that employs trigonometric activation functions. The hidden-layer representation is given by the  $K$ -dimensional complex-valued feature map  $\varsigma(\mathbf{x})$  defined in (8), with the output computed as a linear combination of these components.

Motivated by a prior approach that utilizes intermediate representations from deep neural networks to perform soft clustering of training data in the mixture-of-linear-models framework, we adopt a similar strategy based on the intermediate layer of the RFF model. Specifically, we define the latent space feature representation

$$s(\mathbf{x}) = \text{Re}([\beta_1 e^{i\omega_1 \cdot \mathbf{x}}, \beta_2 e^{i\omega_2 \cdot \mathbf{x}}, \dots, \beta_K e^{i\omega_K \cdot \mathbf{x}}]) \in \mathbb{R}^K,$$

where  $\{\beta_k\}_{k=1}^K$  are the learned weights corresponding to the sampled frequencies  $\{\omega_k\}_{k=1}^K$ . Since accurate approximation of the kernel function under the Monte Carlo scheme typically requires a large value of  $K$ , the resulting features  $s(\mathbf{x})$  are high-dimensional. To facilitate soft clustering based on  $\{s(\mathbf{x}_i)\}_{i=1}^N$ , we apply principal component analysis to reduce the dimensionality from  $K$  to a lower value  $d$ . Empirically, this dimensionality reduction not only improves the robustness of the clustering but also enhances the overall accuracy of the resulting mixture-of-GAM framework. Further implementation details are provided in Section 2.2.

### 2.2. Principal Component Analysis for Feature Extraction

After drawing  $K$  random frequency samples  $\{\omega_k\}_{k=1}^K$  through the RFF model, we construct the intermediate layer representation  $\mathbf{S} \in \mathbb{R}^{N \times K}$ , whose  $(i, k)$ -th entry is given by:

$$\mathbf{S}_{ik} = \operatorname{Re}(\beta_k e^{i\omega_k \cdot \mathbf{x}_i}), \quad \text{for } i = 1, \dots, N, k = 1, \dots, K,$$

where  $\{\beta_k\}_{k=1}^K$  are the trained coefficients and  $\mathbf{x}_i$  denotes the  $i$ -th input data.

To reduce the dimensionality of the high-dimensional representation  $\mathbf{S}$ , we first center it by subtracting the empirical mean across all samples:

$$\bar{\mathbf{S}}_{i,:} = \mathbf{S}_{i,:} - \frac{1}{N} \sum_{i'=1}^N \mathbf{S}_{i',:}, \quad i = 1, \dots, N,$$

where  $\mathbf{S}_{i,:}$  denotes the  $i$ -th row of matrix  $\mathbf{S}$ . This yields a centered matrix  $\bar{\mathbf{S}} \in \mathbb{R}^{N \times K}$ , which is then decomposed using singular value decomposition (SVD) as

$$\bar{\mathbf{S}} = \mathbf{U} \Sigma \mathbf{V},$$

where  $\Sigma \in \mathbb{R}^{N \times K}$  contains the singular values  $\{\sigma_k\}_{k=1}^K$  on its diagonal in descending order,  $\mathbf{V} \in \mathbb{R}^{K \times K}$  contains the right singular vectors (principal directions), and  $\mathbf{U} \in \mathbb{R}^{N \times N}$  contains the left singular vectors representing the projections of the centered data samples  $\bar{\mathbf{S}}$  onto those principal components, as described in Chapter 5.8 of [17].

By selecting the first  $d$  principal components, we obtain a lower-dimensional representation  $\mathbf{Z} \in \mathbb{R}^{N \times d}$  via

$$\mathbf{Z} := \bar{\mathbf{S}} \mathbf{V}_d^\top,$$

where  $\mathbf{V}_d \in \mathbb{R}^{d \times K}$  contains the first  $d$  rows of  $\mathbf{V}$ . This projection captures the most significant variation in the intermediate feature space [19]. In practice, we find that a relatively low-dimensional representation with  $d$  ranging from 2 to 6 suffices to support accurate and robust Gaussian Mixture Model-based soft clustering in the subsequent mixture modeling.

### 2.3. Gaussian Mixture Model for Soft-Clustering

To perform soft clustering on the reduced-dimensional representations  $\{\mathbf{z}_i\}_{i=1}^N$  with  $\mathbf{z}_i \in \mathbb{R}^d$  denoting the  $i$ -th row of matrix  $\mathbf{Z}$ , we fit a Gaussian mixture model with  $L$  components. This approach assumes that the data is generated from a mixture of multivariate Gaussian distributions:

$$p(\mathbf{z}) = \sum_{\ell=1}^L \pi_\ell \mathcal{N}(\mathbf{z}; \boldsymbol{\mu}_\ell, \boldsymbol{\Sigma}_\ell),$$

where  $\pi_\ell \in [0, 1]$  denotes the weight of the  $\ell$ -th component, satisfying  $\sum_{\ell=1}^L \pi_\ell = 1$ , and each component  $\mathcal{N}(\mathbf{z}; \mu_\ell, \Sigma_\ell)$  is a multivariate normal distribution with mean  $\mu_\ell \in \mathbb{R}^d$  and covariance matrix  $\Sigma_\ell \in \mathbb{R}^{d \times d}$ .

The model parameters  $\pi_\ell$ ,  $\mu_\ell$ , and  $\Sigma_\ell$  for  $\ell = 1, \dots, L$  are estimated via the *Expectation-Maximization* (EM) algorithm. The EM algorithm iteratively estimates the posterior responsibilities and updates the model parameters to maximize the likelihood of the observed data. With given fitting parameters, the *posterior responsibility* (i.e., the soft cluster assignment) of the  $\ell$ -th component for a given point  $\mathbf{z} \in \mathbb{R}^d$  is computed by:

$$\gamma_\ell(\mathbf{z}) := \frac{\pi_\ell \mathcal{N}(\mathbf{z}; \mu_\ell, \Sigma_\ell)}{\sum_{\ell'=1}^L \pi_{\ell'} \mathcal{N}(\mathbf{z}; \mu_{\ell'}, \Sigma_{\ell'})}.$$

These posterior weights  $\{\gamma_\ell(\mathbf{z})\}_{\ell=1}^L$  serve for the subsequent construction of the mixture-of-GAM framework. Further details on Gaussian mixture models and the EM algorithm can be found in [4, 11].

#### 2.4. Generalized Additive Models with Interpretability

To model the regression structure within each cluster, we adopt the framework of Generalized Additive Models [18, 20, 42]. Let

$$\{(\mathbf{x}_i, y_i)\}_{i=1}^{N_\ell}, \quad \ell = 1, \dots, L, \quad \text{with } \sum_{\ell=1}^L N_\ell = N,$$

denote the partition of the training data obtained from GMM-based clustering on the RFF-derived latent representation. Within each cluster  $\ell$ , the conditional mean of the response is modeled as an additive function

$$\tilde{f}^{(\ell)}(\mathbf{x}) = \alpha^{(\ell)} + \sum_{j=1}^p g_j^{(\ell)}(x_j),$$

where  $\alpha^{(\ell)}$  is the intercept and each  $g_j^{(\ell)}(x_j)$  is a smooth univariate function representing the effect of the  $j$ -th predictor variable  $x_j$ .

Each component function  $g_j^{(\ell)}$  is represented using a *B-spline basis* [5] expansion

$$g_j^{(\ell)}(x_j) = \sum_{q=1}^{Q_j} \theta_{j,q}^{(\ell)} \phi_{j,q}(x_j),$$

where  $\{\phi_{j,q}\}_{q=1}^{Q_j}$  are B-spline basis functions constructed with quantile-based interior knots, and  $\theta_{j,q}^{(\ell)} \in \mathbb{R}$  are the corresponding coefficients, which are estimated by minimizing a cluster-specific penalized least-squares criterion. For cluster  $\ell$ , the objective function is

$$\min_{\alpha^{(\ell)}, \{\theta_{j,q}^{(\ell)}\}} \left\{ \sum_{i=1}^{N_\ell} \left( y_i - \alpha^{(\ell)} - \sum_{j=1}^p g_j^{(\ell)}(x_{ij}) \right)^2 + \lambda \sum_{j=1}^p \int (g_j^{(\ell)''}(t))^2 dt \right\},$$

where  $\lambda > 0$  controls the smoothness of the estimated functions. In practice, the roughness penalty is implemented through a quadratic form

$$\int (g_j''(t))^2 dt \approx (\theta_j^{(\ell)})^\top \Omega_j \theta_j^{(\ell)},$$

where  $\Omega_j$  is constructed from second-order finite-difference operators on the spline basis.

Because the optimization is additive in the component functions, we employ the classical *back-fitting algorithm* [18] which iteratively updates each  $g_j^{(\ell)}$  by smoothing its partial residual against covariate  $x_j$ , holding all other components fixed. This reduces the multivariate smoothing problem to a sequence of one-dimensional penalized regressions.

The additive structure within each cluster facilitates model-based interpretability, as each component function  $g_j^{(\ell)}$  isolates the marginal effect of a single predictor variable  $x_j$  of cluster  $\ell$ , consistent with the interpretability properties of GAMs discussed in [18]. The resulting effects can be visualized through a *partial dependence plot* [16], which is a widely used tool for examining feature influence in both additive and more general predictive models. Further details regarding our numerical implementation are provided in Section 4.1.1.

### 3. Method

The complete workflow of our mixture-of-GAMs model consists of four main stages:

#### 1. Random Fourier feature model training.

Train a random Fourier feature model

$$\bar{m}(\mathbf{x}) = \boldsymbol{\beta}^\top \varsigma(\mathbf{x}) = \sum_{k=1}^K \beta_k e^{i\omega_k \cdot \mathbf{x}},$$

on the input training data  $\{(\mathbf{x}_i, y_i)\}_{i=1}^N$  to approximate the target regression function, which yields a high-dimensional hidden-layer representation  $\mathbf{S} \in \mathbb{R}^{N \times K}$  with matrix elements

$$\mathbf{S}_{ik} = \text{Re}(\beta_k e^{i\omega_k \cdot \mathbf{x}_i}), \quad i = 1, \dots, N, \quad k = 1, \dots, K,$$

based on sampled frequencies  $\{\omega_k\}_{k=1}^K$  and trained coefficients  $\{\beta_k\}_{k=1}^K$ .

#### 2. Dimensionality reduction and GMM-based soft clustering.

Compute the sample mean  $\bar{\mathbf{s}} = \frac{1}{N} \sum_{i=1}^N \mathbf{S}_{i,:}$  of the intermediate feature representation  $\mathbf{S}$ , and apply principal component analysis on the centered matrix  $\bar{\mathbf{S}}$  via singular value decomposition  $\bar{\mathbf{S}} = \mathbf{U} \boldsymbol{\Sigma} \mathbf{V}$  to obtain the lower-dimensional representation

$$\mathbf{Z} = \bar{\mathbf{S}} \mathbf{V}_d^\top,$$

where  $\mathbf{V}_d \in \mathbb{R}^{d \times K}$  contains the first  $d$  principal directions of the right singular matrix  $\mathbf{V}$ . The resulted reduced data representation  $\mathbf{Z} \in \mathbb{R}^{N \times d}$  allows the fitting of a Gaussian Mixture Model

$$p(\mathbf{z}) = \sum_{\ell=1}^L \pi_\ell \mathcal{N}(\mathbf{z}; \boldsymbol{\mu}_\ell, \boldsymbol{\Sigma}_\ell),$$

which for a latent space representation  $h(\mathbf{x}) : \mathbb{R}^p \rightarrow \mathbb{R}^d$  provides the soft clustering responsibilities

$$\gamma_\ell(\mathbf{x}) = \frac{\pi_\ell \mathcal{N}(h(\mathbf{x}); \mu_\ell, \Sigma_\ell)}{\sum_{\ell'=1}^L \pi_{\ell'} \mathcal{N}(h(\mathbf{x}); \mu_{\ell'}, \Sigma_{\ell'})}, \quad \ell = 1, \dots, L, \quad (12)$$

where

$$h(\mathbf{x}) := \mathbf{V}_d (s(\mathbf{x}) - \bar{\mathbf{s}}), \quad \text{with } s(\mathbf{x}) := \text{Re}(\boldsymbol{\beta} \odot \varsigma(\mathbf{x})) \in \mathbb{R}^K.$$

### 3. Fitting local generalized additive models.

Assign each training data point to a cluster based on the maximum posterior responsibility. For each cluster  $\{(\mathbf{x}_i, y_i)\}_{i=1}^{N_\ell}$ , train a local generalized additive model

$$\tilde{f}^{(\ell)}(\mathbf{x}) = \alpha^{(\ell)} + \sum_{j=1}^p g_j^{(\ell)}(x_j), \quad \ell = 1, \dots, L,$$

on the corresponding subset of training data, where each component function  $g_j^{(\ell)}(x_j)$  uses B-spline basis functions with quantile-based knots.

### 4. Constructing the final mixture model.

Use the posterior responsibilities  $\gamma_\ell(\mathbf{x})$  from the GMM to compute a weighted combination of the predictions by the local GAMs. This defines the final mixture-of-GAMs regression model

$$\tilde{m}(\mathbf{x}) = \sum_{\ell=1}^L \gamma_\ell(\mathbf{x}) \tilde{f}^{(\ell)}(\mathbf{x}).$$

The overall workflow of the proposed mixture-of-GAM framework is summarized in Algorithm 1 and visually illustrated in Figure 1. To provide a more explicit visualization of the data matrices, feature construction, and latent-space clustering, Figure 2 presents an extended diagram including the graphical representations used throughout the pipeline.

## 4. Numerical Experiment

To numerically validate the proposed mixture-of-GAMs framework, we apply Algorithm 1 to four benchmark regression datasets: the California Housing dataset [26], the Airfoil Self-Noise dataset [7], the Bike Sharing dataset [13], and the Kin40k dataset [30]. Across these datasets, we compare the proposed approach with a range of baseline models spanning both classical statistical methods and modern machine learning techniques. The baselines include random Fourier feature (RFF) regression with resampling-based frequency optimization [21], a global generalized additive model (GAM, [18]), least absolute shrinkage and selection operator (LASSO, [40]), multivariate adaptive regression splines (MARS, [15]), Random Forest [6], XGBoost [9], Explainable Boosting Machine [8, 25], multilayer perceptron (MLP, [35]), and mixture-of-linear-models (MLM, [38]). These methods are grouped into three categories: highly expressive but less directly interpretable models (MLP, Random Forest, XGBoost, and RFF), standard interpretable regression approaches (LASSO, MARS, Explainable Boosting Machine, and the global GAM), and locally adaptive mixture models based on either linear components (MLM) or generalized additive components (mixture-of-GAMs).

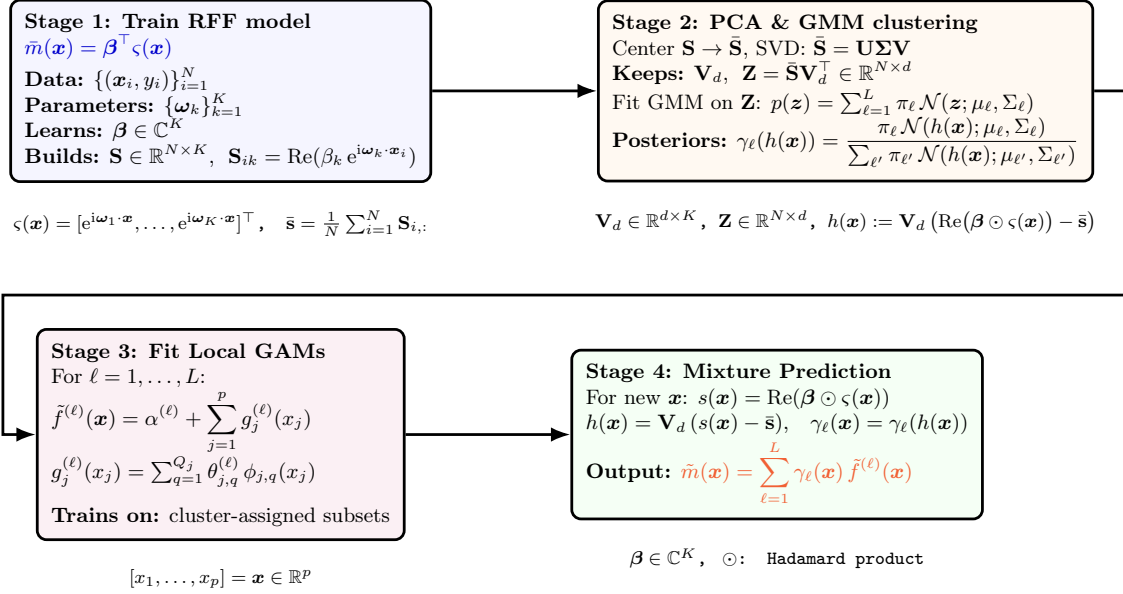


Figure 1: The overall pipeline of the RFF-informed mixture-of-GAMs. Stage 1 learns RFF model coefficients and builds a random Fourier feature space representation. Stage 2 reduces to a lower-dimensional representation via PCA and fits a GMM to obtain posterior responsibilities. Stage 3 trains local GAMs for each cluster of the training dataset. Stage 4 forms the final prediction.

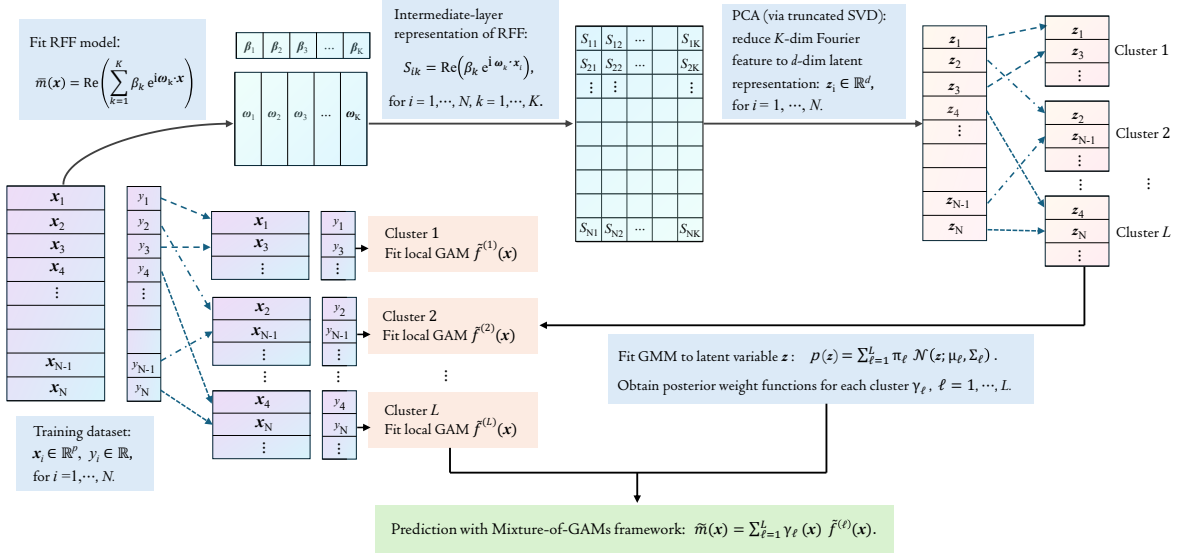


Figure 2: Diagram with graphical representations of the workflow of the mixture-of-GAMs method informed with random Fourier features.

---

**Algorithm 1** Training Pipeline for RFF-informed Mixture-of-GAMs

---

- 1: **Input:** Training data  $\{(\mathbf{x}_i, y_i)\}_{i=1}^N$ , number of Fourier features  $K$ , reduced dimension  $d$ , number of clusters  $L$
- 2: **Output:** Trained local GAM models  $\{\tilde{f}^{(\ell)}(\mathbf{x})\}_{\ell=1}^L$  and posterior weight functions  $\{\gamma_\ell(\mathbf{x})\}_{\ell=1}^L$
- 3: **Stage 1: Training of Random Fourier Feature model**
  - Sample frequency parameters  $\{\omega_k\}_{k=1}^K \sim \rho(\omega)$
  - Construct feature mapping  $\varsigma(\mathbf{x}) := [e^{i\omega_1 \cdot \mathbf{x}}, \dots, e^{i\omega_K \cdot \mathbf{x}}]^\top$
  - Train the RFF regression model  $\bar{m}(\mathbf{x}) = \boldsymbol{\beta}^\top \varsigma(\mathbf{x})$
  - Define intermediate feature vector  $s(\mathbf{x}) := \text{Re}(\boldsymbol{\beta} \odot \varsigma(\mathbf{x}))$
  - Build intermediate feature matrix  $\mathbf{S} \in \mathbb{R}^{N \times K}$  by stacking rows  $s(\mathbf{x}_i)^\top$  for  $i = 1, \dots, N$
- 4: **Stage 2: Dimensionality Reduction and GMM-based Clustering**
  - Obtain centered feature matrix  $\bar{\mathbf{S}}$  by subtracting from each row of  $\mathbf{S}$  the empirical mean  $\bar{\mathbf{s}} = \frac{1}{N} \sum_{i=1}^N \mathbf{S}_{i,:}$
  - Apply PCA via SVD:  $\bar{\mathbf{S}} = \mathbf{U} \boldsymbol{\Sigma} \mathbf{V}^\top$ , retain first  $d$  principal directions  $\mathbf{V}_d$
  - Compute reduced representation:  $\mathbf{Z} = \bar{\mathbf{S}} \mathbf{V}_d^\top \in \mathbb{R}^{N \times d}$
  - Fit GMM on  $\mathbf{Z}$  to obtain cluster weights  $\{\pi_\ell\}_{\ell=1}^L$ , means  $\{\mu_\ell\}_{\ell=1}^L$ , and covariances  $\{\Sigma_\ell\}_{\ell=1}^L$
  - Derive posterior responsibilities  $\gamma_\ell(\mathbf{x}) = \frac{\pi_\ell \mathcal{N}(h(\mathbf{x}); \mu_\ell, \Sigma_\ell)}{\sum_{\ell'=1}^L \pi_{\ell'} \mathcal{N}(h(\mathbf{x}); \mu_{\ell'}, \Sigma_{\ell'})}$  for  $\ell = 1, \dots, L$ , where  $h(\mathbf{x}) = \mathbf{V}_d(s(\mathbf{x}) - \bar{\mathbf{s}})$
- 5: **Stage 3: Training of Local GAMs**

For each  $\ell = 1, \dots, L$ :

  - Select training data points with the highest posterior responsibility for cluster  $\ell$
  - Fit local GAM:  $\tilde{f}^{(\ell)}(\mathbf{x}) = \alpha^{(\ell)} + \sum_{j=1}^p g_j^{(\ell)}(x_j)$  on each covariate dimension  $j = 1, \dots, p$ , using B-spline basis with quantile-based knots
- 6: **Stage 4: Mixture-of-GAMs Prediction**

For a new input  $\mathbf{x}$ :

  - Compute  $s(\mathbf{x}) = \text{Re}(\boldsymbol{\beta} \odot \varsigma(\mathbf{x}))$
  - Compute reduced representation  $h(\mathbf{x}) = \mathbf{V}_d(s(\mathbf{x}) - \bar{\mathbf{s}})$
  - Evaluate responsibilities  $\{\gamma_\ell(h(\mathbf{x}))\}_{\ell=1}^L$
  - Predict:
$$\tilde{m}(\mathbf{x}) = \sum_{\ell=1}^L \gamma_\ell(h(\mathbf{x})) \tilde{f}^{(\ell)}(\mathbf{x})$$


---

#### 4.1. California Housing Dataset

The California Housing dataset contains 20640 samples with eight continuous predictor variables: latitude, longitude, median house age, average number of rooms, average number of bedrooms, block population, average house occupancy, and median income. The target variable is the median house

value (in USD) for each census block group in California, as recorded in the 1990 U.S. Census. In our experiments, the dataset is randomly split into training and test sets, using 80% of the data for training and the remaining 20% for evaluation.

#### 4.1.1. Mixture-of-GAMs guided by the complete random Fourier feature model

We begin by training a random Fourier feature model using a resampling-based scheme designed to improve the efficiency of frequency selection, guided by the empirical covariance structure of the frequency samples [21]. In the numerical experiments, the number of random Fourier features  $K$  is selected by gradually increasing  $K$  until the validation performance stabilizes, indicating that the approximation error due to finite random features is no longer the dominant source of error. Specifically for this dataset, a total of  $K = 4000$  random frequency samples are generated. The convergence behavior of the model, measured by training and test error over successive resampling iterations, is presented in Figure 3.

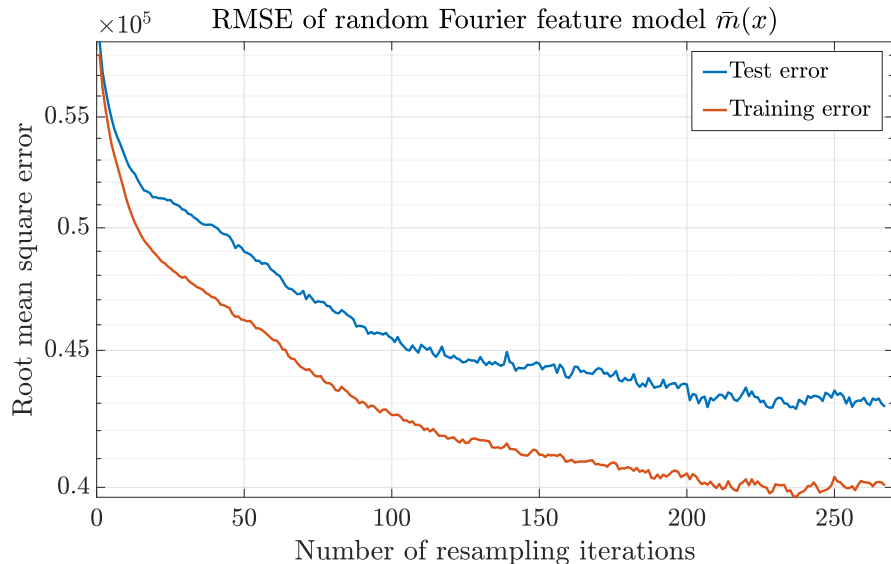


Figure 3: Root mean square error of the trained random Fourier feature model  $\bar{m}(\mathbf{x})$ , with increasing number of resampling iterations on the random frequency samples.

Table 1 summarizes the predictive performance of several statistical and machine-learning models on the California housing dataset. All RMSE values reported in Table 1 are scaled in units of  $10^5$  USD.

Within the first group of highly expressive but less interpretable models, the resampling-based random Fourier feature regression model attains a test RMSE ( $0.439 \pm 0.021$ ) that is statistically comparable to that of XGBoost ( $0.437 \pm 0.021$ ), while outperforming both the Random Forest and MLP. This performance suggests that the Fourier feature representation captures the dominant structure of the data more effectively than the bootstrap-aggregated decision-tree ensemble or the fully learned embedding of a deep neural network, enabling competitive accuracy with state-of-the-art gradient-boosted ensembles.

Table 1: Comparison of root mean square error (RMSE) on the training and test sets of the California Housing dataset for multiple model classes, including highly expressive but less interpretable predictive models (RFF, MLP, Random Forest), standard interpretable models (LASSO, MARS, global GAM, Explainable Boosting Machine), and locally adaptive mixtures (MLM and mixture of GAMs). Reported uncertainties denote 95% confidence intervals obtained via bootstrap resampling of the test residuals with 1000 resamples.

Model	Training RMSE	Test RMSE
MLP	0.503	$0.517 \pm 0.035$
Random Forest	0.181	$0.502 \pm 0.023$
XGBoost	0.236	$0.437 \pm 0.021$
RFF model	0.396	$0.439 \pm 0.021$
LASSO	0.726	$0.723 \pm 0.023$
MARS	0.629	$0.640 \pm 0.022$
Global GAM	0.548	$0.567 \pm 0.023$
Explainable Boosting Machine	0.453	$0.489 \pm 0.023$
MLM-cell	0.560	$0.570 \pm 0.031$
MLM-epic	0.569	$0.584 \pm 0.032$
Mixture of GAMs with complete RFF	0.461	$0.501 \pm 0.022$
Mixture of GAMs with spatial RFF	0.442	$0.489 \pm 0.021$

Standard interpretable baselines, including LASSO, MARS, the global GAM, and the Explainable Boosting Machine, demonstrate a consistent progression in accuracy as model flexibility increases, with the Explainable Boosting Machine achieving the strongest performance in this group. By extending the global GAM framework into a locally adaptive mixture, the proposed approach further addresses data heterogeneity by permitting local specialization through clustering within the informative latent space derived from Fourier features. Both mixture-of-GAMs variants outperform the global GAM and the two MLM baselines, illustrating the advantage of combining Fourier-based spectral representations with smooth, interpretable nonlinear components. Notably, the mixture of GAMs constructed using spatial Fourier features achieves the best performance within the mixture model family and is statistically competitive with Explainable Boosting Machine (0.489 test RMSE for both). This result indicates that clustering informed by geographic structure is particularly effective for capturing the underlying patterns of the California housing dataset. Implementation details and hyperparameter settings for the proposed Mixture-of-GAMs framework and baseline models are provided in Appendix A.

To assess the effect of two key hyperparameters: the number of clusters  $L$  in the mixture model and the dimension  $d$  of the PCA-projected RFF representation, we conduct a grid search over values of  $(L, d)$  with range  $L = 3, \dots, 8$  and  $d = 2, \dots, 8$ . For each pair, we train the mixture-of-GAMs model on the training data and evaluate the test RMSE on the fixed held-out test set. The results are visualized in a heatmap, where each grid cell displays the corresponding RMSE value, as shown in Figure 4.

To further evaluate the behavior of the trained mixture-of-GAMs model, we visualize the partial dependence functions, defined for each feature  $x_j$  as

$$\text{PD}_j(x_j) := \frac{1}{N} \sum_{i=1}^N \bar{m}(x_j, \mathbf{x}_{i,-j}),$$

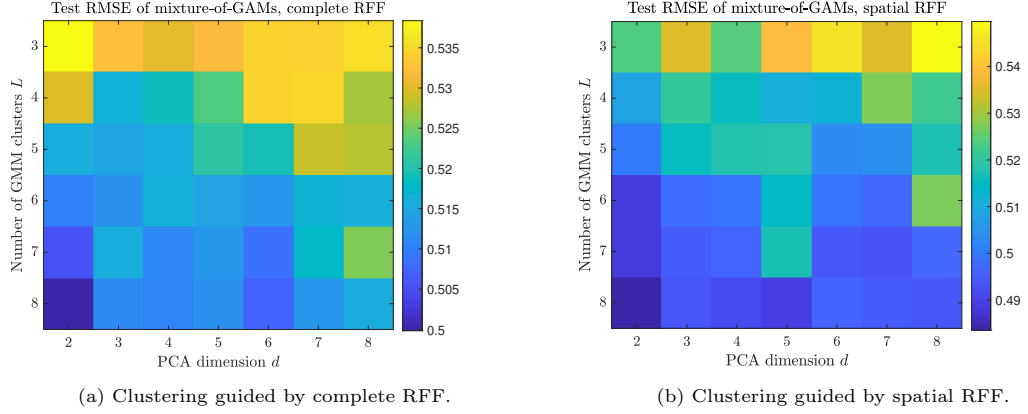


Figure 4: Test root mean square error on California housing dataset evaluated over a grid of hyperparameter configurations  $(L, d)$ , where  $L$  is the number of mixture components and  $d$  is the number of retained principal components after PCA on the intermediate feature representations. Panel (a) uses the full set of RFF features to guide the Gaussian mixture model-based clustering, while panel (b) relies solely on spatial RFF features derived from geographic coordinates.

where  $\mathbf{x}_{i,-j} \in \mathbb{R}^{p-1}$  is the vector of all covariates except  $x_j$ , taken from the  $i$ -th training sample. For each fixed value of  $x_j$ , we evaluate the model at points  $(x_j, \mathbf{x}_{i,-j})$  for all  $i = 1, \dots, N$ , and the results are averaged to yield the partial dependence curve:  $x_j \mapsto \text{PD}_j(x_j)$ .

Figure 5 displays the partial dependence plots of the trained mixture-of-GAMs model (in violet) for six selected predictor variables: median house age, average number of rooms, average number of bedrooms, block population, average house occupancy, and median income. For comparison, the corresponding curves from the trained RFF model (in blue) and the global GAM model (in red) are also shown. The mixture-of-GAMs curves exhibit a similar trend and closer agreement with those of the RFF model, reflecting the fact that the RFF-based feature extraction effectively informs the mixture framework.

#### 4.1.2. Mixture of GAMs guided by spatial Fourier features

If we restrict the RFF input to only the spatial coordinates  $(\xi_i, \eta_i)_{i=1}^N$ , obtained by converting the longitude and latitude values in the California housing dataset, then, since the RFF model uses frequency vectors  $\omega_k, k = 1^K$  with  $\omega_k = (\omega_{k,\xi}, \omega_{k,\eta}) \in \mathbb{R}^2$ , corresponding to sinusoidal variations along different spatial directions, the resulting mixture components correspond directly to spatial locations. Consequently, we can immediately associate the local GAM models with geographic regions, yielding a desirable and intuitive form of interpretation. Next, we investigate this approach and evaluate its predictive accuracy.

Despite using only two spatial covariates, the resulting simpler spatial RFF model achieves a test RMSE of  $0.56 \times 10^5$  USD. We then apply PCA to the intermediate features  $\mathbf{S} \in \mathbb{R}^{N \times K}$  with elements

$$\mathbf{S}_{ik} = \text{Re} \left( \beta_k e^{i(\xi_i \omega_{k,\xi} + \eta_i \omega_{k,\eta})} \right), \quad i = 1, \dots, N, \text{ and } k = 1, \dots, K,$$

produced by the RFF layer, and use the reduced-dimensional representation to perform GMM-based clustering on the training data. Figures 6 and 7 show the spatial distribution of data points in each cluster, allowing for a visual comparison between the clustering based on spatial features and that

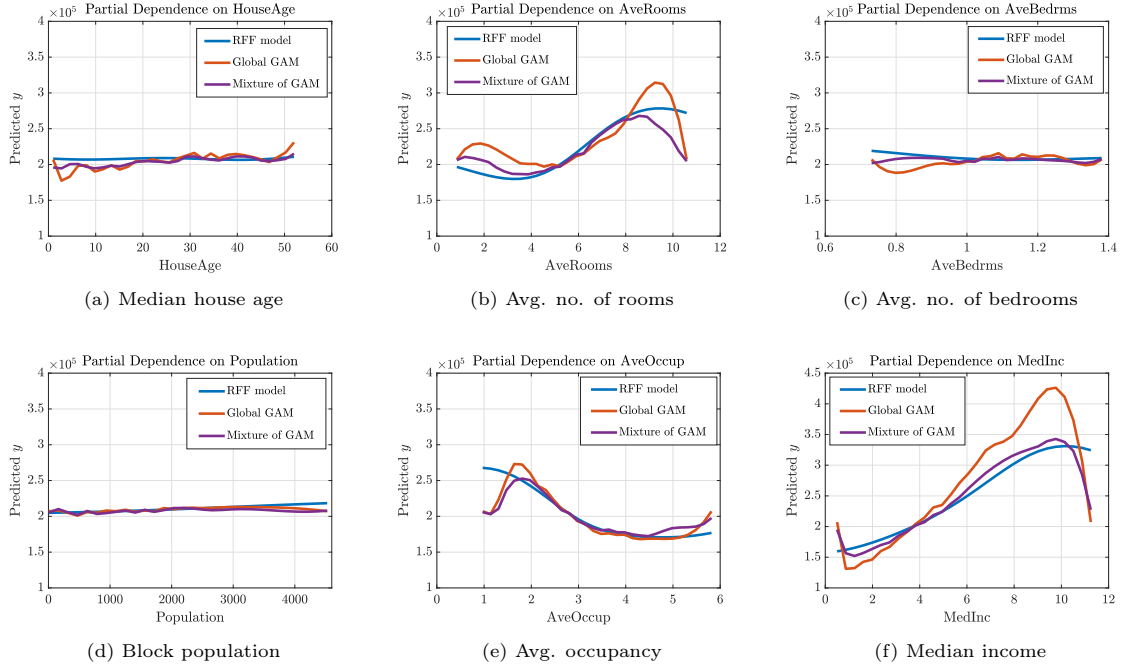


Figure 5: Partial dependence plots for selected features of the California Housing dataset.

derived using all covariates. We observe that the clusters form stripe-like patterns roughly parallel to the California coastline. This structure is consistent with the state's economic development pattern: as one moves inland from the coast, the cost of living generally decreases, whereas along the coastline there is relatively slight variation from northwest to southeast.

We further examine the learned spatial structure by plotting the empirical histogram of the two-dimensional frequency samples  $\{(\omega_{k,\xi}, \omega_{k,\eta})\}_{k=1}^K$  in Figure 9b. California's coastline runs approximately from northwest to southeast, while the inland direction (which roughly points from southwest to northeast) is associated with the systematic decline in housing prices as distance from major coastal cities increases, as illustrated in Figure 9a. To quantify the dominant orientation in the learned frequency distribution, we apply a weighted PCA based on *kernel density estimates*, computed using the classical Rosenblatt-Parzen formulation [27, 33]. This weighting emphasizes the high-density core of the distribution. The resulting principal direction (denoted by  $v_1$  in Figures 9a and 9b) aligns closely with the inland-coastal gradient observed in the housing price data. This agreement indicates that the spatial RFF model, in conjunction with the resampling algorithm presented in [21], successfully captures the primary axis of geographic variation and directly extracts meaningful large-scale spatial structure from the data.

This observation can be heuristically understood through the relationship between kernel smoothness and its Fourier transform. If the target function varies more strongly along a certain spatial direction (here, the inland direction), sharper kernels are needed to approximate these fluctuations. Since the Fourier transform of the Gaussian RBF kernel defined in (4) has spectral variance proportional to  $1/\sigma^2$ , where  $\sigma$  denotes the kernel width (standard deviation), this translates into allocating more high-frequency components in the same direction. This behavior is illustrated in Figure 8,

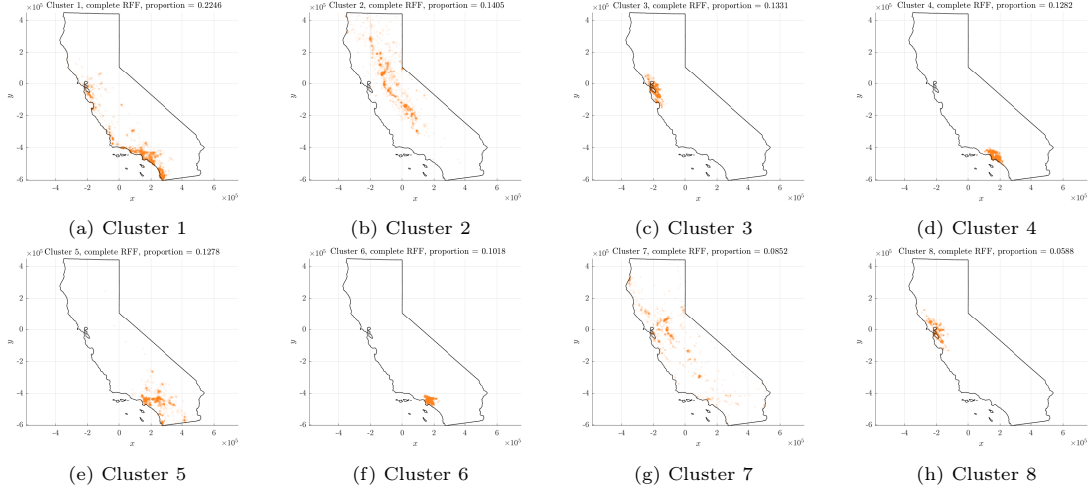


Figure 6: Spatial distributions of training data for each GMM cluster in the California housing dataset, using complete random Fourier features.

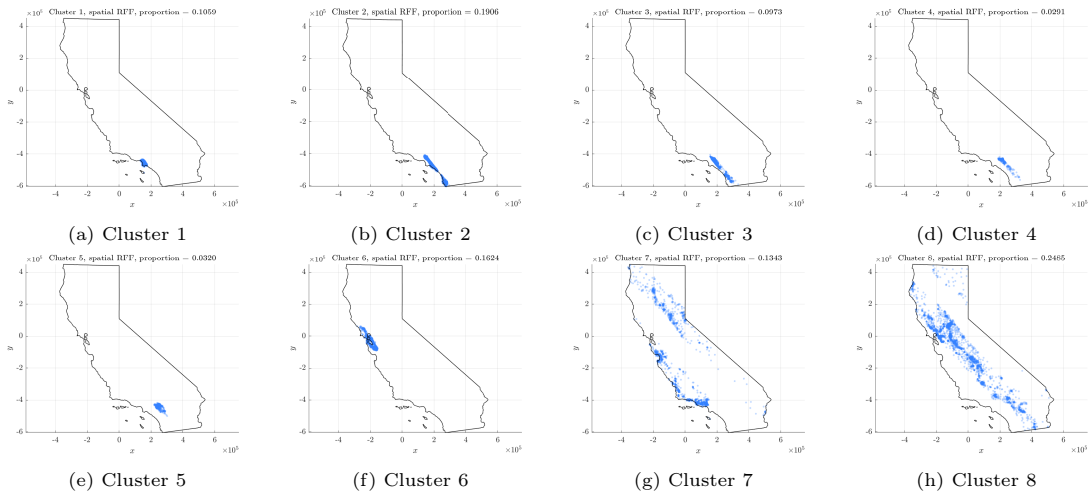


Figure 7: Spatial distributions of training data for each GMM cluster in the California housing dataset, based on explainable spatial Fourier features.

which shows how a Gaussian kernel with a narrower width in the spatial domain corresponds to a broader spread in its Fourier spectrum. Conversely, in directions with weaker variation, the frequency distribution is more concentrated near the low-frequency region. This intuition is consistent with the observed anisotropy of the learned frequency samples.

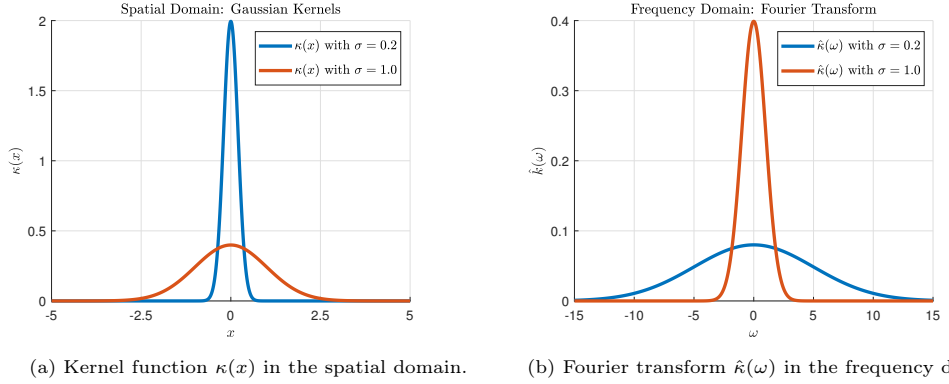


Figure 8: Illustration of the inverse relation between the spatial and spectral scales of Gaussian kernels. Left: Gaussian kernels with different band width parameters  $\sigma$  in the spatial domain. Right: Corresponding normalized Fourier transforms, showing broader spectral spread for smaller  $\sigma$ .

Based on the learned spatial Fourier features  $\{(\omega_{k,\xi}, \omega_{k,\eta})\}_{k=1}^K$  and the associated amplitudes  $\{\beta_k\}_{k=1}^K$ , we apply GMM-based clustering on the principal components of intermediate feature representation and subsequently train the corresponding cluster-wise GAM models. The resulting mixture-of-GAMs framework achieves a test RMSE of  $0.489 \times 10^5$  USD, which is comparable to the performance obtained when clustering is guided by the full random Fourier features over all eight covariates ( $0.501 \times 10^5$  USD), as reported in the last two rows of Table 1.

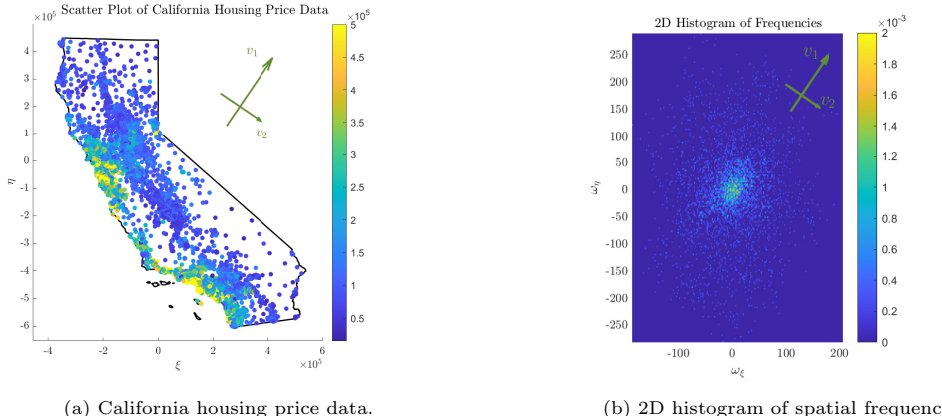


Figure 9: Plot of California housing price data (left) and 2D empirical histogram of frequency samples  $\{(\omega_{k,\xi}, \omega_{k,\eta})\}_{k=1}^K$  (right). In both panels,  $v_1$  denotes the principal direction of variation identified by the weighted PCA of the frequency samples, and  $v_2$  denotes the orthogonal direction.

#### 4.2. Airfoil Self-Noise Dataset

The Airfoil Self-Noise dataset, derived from a series of NASA wind-tunnel experiments, contains 1503 samples describing aerodynamic noise generated by airfoils under varying operating conditions. The five continuous predictor variables are: frequency, angle of attack, chord length, free-stream velocity, and suction-side displacement thickness. The target variable is the scaled sound pressure level of the airfoil, expressed in decibels (dB).

Compared to the California Housing dataset, the Airfoil Self-Noise dataset is smaller in sample size and has relatively sparse coverage of the covariate space, making it more challenging for models with a large number of parameters to avoid overfitting. Moreover, the underlying physical relationships among the variables may be nonlinear and coupled, which further complicates modeling. Figure 10 illustrates the empirical distributions of the five predictor variables based on their histograms. Because the frequency variable spans several orders of magnitude, we apply a logarithmic transformation to stabilize its scale before fitting the model.

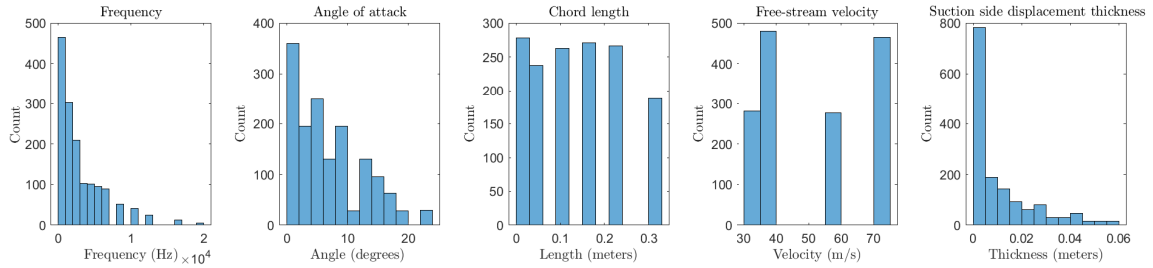


Figure 10: Histograms of the five covariates in the Airfoil Self-Noise dataset.

With a reduced dimension of  $d = 3$  and  $L = 12$  clusters, the mixture-of-GAMs framework attains a test RMSE of approximately 2.2 dB on the Airfoil Self-Noise dataset, significantly improving upon the global GAM ( $4.51 \pm 0.08$  dB) and MARS ( $4.98 \pm 0.08$  dB). Within the group of highly expressive models, the resampling-based RFF model ( $1.08 \pm 0.02$  dB) outperforms both XGBoost ( $1.43 \pm 0.03$  dB) and Random Forest ( $1.60 \pm 0.03$  dB), demonstrating the superior representational capacity of adaptive Fourier features for this aerodynamic task. By using  $K = 2000$  random Fourier features with the resampling strategy, the RFF model attains an accuracy that is highly comparable to the state-of-the-art performance (test RMSE 1.2–1.5 dB) achieved by a *hybrid CatBoost-AOA* approach, as reported in [31].

The mixture-of-GAMs framework substantially outperforms the global GAM, highlighting the critical role of local specialization in capturing the dataset's underlying physical complexities. Notably, the framework achieves an accuracy that is statistically competitive to the Explainable Boosting Machine (2.2 dB test RMSE for both). This performance is primarily driven by the RFF-based clustering's ability to uncover distinct latent data regimes, which allows the subsequent local GAMs to model nonlinear univariate effects with a level of precision that global interpretable models cannot match.

Figure 11 presents the partial dependence plots for the five predictor variables of the Airfoil Self-Noise dataset. Across most variables, including acoustic frequency, angle of attack, chord length, and free-stream velocity, the mixture-of-GAMs model (violet) aligns more closely with the RFF model (blue) than the global GAM (red). For displacement thickness, both models show similarly limited agreement with the RFF reference, though the mixture of GAMs displays slightly

Table 2: Comparison of root mean square error (RMSE) on the training and test sets of the Airfoil Self-Noise dataset across six models: Random Forest, RFF, LASSO, MARS, global GAM, and locally adaptive mixture of GAMs trained on the original and RFF-augmented datasets.

Model	Training RMSE	Test RMSE
Random Forest	0.68	$1.60 \pm 0.03$
XGBoost	0.36	$1.43 \pm 0.03$
RFF model	0.67	$1.08 \pm 0.02$
LASSO	4.79	$4.82 \pm 0.09$
MARS	4.95	$4.98 \pm 0.08$
Global GAM	4.45	$4.51 \pm 0.08$
Explainable Boosting Machine	1.38	$2.21 \pm 0.04$
Mixture of GAMs (original data)	2.01	$2.22 \pm 0.05$
Mixture of GAMs (augmented data)	1.84	$2.02 \pm 0.04$

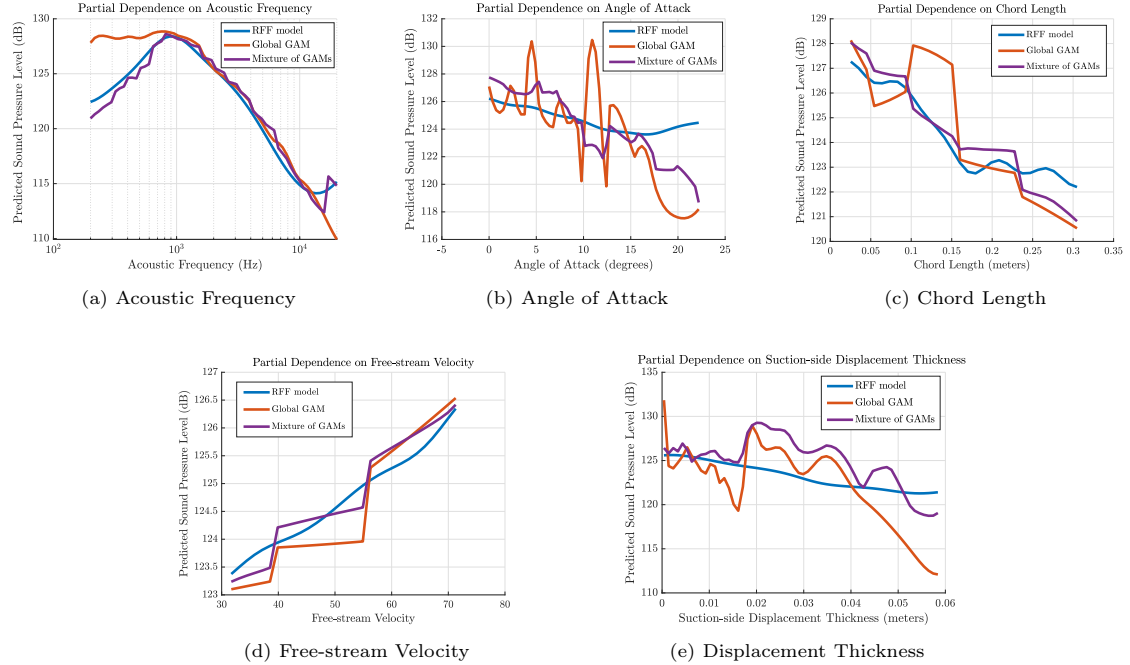


Figure 11: Partial dependence plots on the five covariates of the Airfoil Self-noise dataset.

better alignment in certain regions. Overall, these comparisons indicate that the mixture of GAMs generally corresponds more closely to the RFF reference than the single global GAM, in line with the test RMSE results in Table 2.

In addition to training on the original dataset, we also experiment with a data-augmentation strategy in which new covariate vectors are generated by applying Gaussian perturbations to the standardized training data. Specifically, for each standardized training sample  $\mathbf{x}$ , we draw ten

independent perturbations from a multivariate normal distribution  $\Delta\mathbf{x} \sim \mathcal{N}(0, \epsilon I)$  with  $\epsilon = 0.05$ , and form simulated candidates as  $\tilde{\mathbf{x}} = \mathbf{x} + \Delta\mathbf{x}$ . This procedure follows the perturbation-based data-augmentation approach used in the mixture-of-linear-models framework [38].

To ensure the plausibility of the simulated covariates, we filter the perturbed candidates using a Mahalanobis-distance threshold calibrated by the 99% chi-squared quantile (see Chapter 3.2 of [23]). This removes points that fall outside a high-confidence ellipsoid of the empirical distribution and retains only those lying near the estimated data manifold. The accepted synthetic covariate vectors are then assigned labels using predictions from the previously trained RFF model and combined with the original dataset to form an augmented training set. The enriched dataset is then used to re-fit the Gaussian mixture model for clustering, enabling the resulting mixture-of-GAMs formulation to better capture structural patterns in the covariate space. As summarized in Table 2, this perturbation-based augmentation strategy improves test RMSE from 2.2 dB to 2.0 dB on the Airfoil Self-Noise dataset when using a reduced dimension  $d = 3$  and  $L = 12$  mixture components, leading to a relative improvement of about 9%.

To evaluate the predictive uncertainty, we use *repeated training/test splits method* (also known as *Monte Carlo cross-validation*, see Chapter 4 of [22]), in which the dataset is repeatedly and independently split into training and test subsets, and performance metrics are averaged across repetitions. Using 100 Monte Carlo repetitions, we estimate the mean RMSE and report the associated 95% confidence interval.

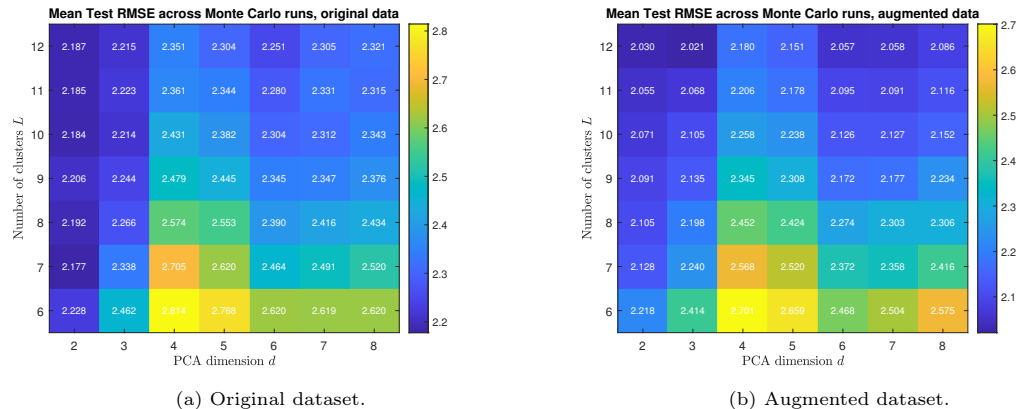


Figure 12: Test root mean square error on the airfoil self-noise dataset evaluated over a grid of hyperparameter configurations  $(L, d)$ , where  $L$  is the number of mixture components and  $d$  is the number of retained PCA components. Panel (a) uses the original dataset, while panel (b) uses the RFF-augmented dataset.

Hyperparameters  $L$  and  $d$  are selected via the grid search method (as in Section 4.1). Figure 12 shows the RMSE surfaces over  $(L, d)$ -pairs for both original and augmented datasets. The augmented variant clearly exhibits improved performance across a broader range of configurations.

To disentangle the contributions of the clustering representation and the expressiveness of the local predictive models, we conduct a targeted ablation study on the California Housing and Airfoil Self-Noise datasets. Specifically, we compare clustering based on raw input features, PCA-reduced inputs, and further examine the effect of replacing local generalized additive models by linear models under identical RFF-induced clustering assignments. Across both datasets, clustering in the RFF-based representation consistently yields improved predictive performance relative to unsupervised

input-space alternatives, while local GAMs provide additional gains over linear models within the same clusters. These results confirm that both the choice of clustering representation and the non-linear local model class contribute meaningfully to the performance of the proposed framework. Full experimental details and numerical results are reported in Appendix B.

#### 4.3. Bike Sharing Dataset

The Bike Sharing dataset contains 17379 hourly observations of bicycle rental counts from a public bike-sharing system in Washington, D.C., collected over the period 2011–2012. The response variable is the total number of rentals per hour. The predictors comprise temporal variables (year, month, day of week, and hour of day), meteorological covariates (temperature, apparent temperature, humidity, and wind speed), and several binary or categorical indicators, including working-day, holiday, season, and weather condition, which encode discrete contextual effects on demand.

Compared with the California Housing and Airfoil Self-Noise datasets, the Bike Sharing dataset exhibits greater structural heterogeneity, arising from the interaction between smooth meteorological effects and discrete temporal or categorical regimes, such as commuting versus leisure hours or seasonal usage patterns. At the same time, the dependence on continuous meteorological variables is largely smooth and approximately monotone, suggesting that locally linear or mildly nonlinear models may already capture a substantial portion of the predictive structure, provided that temporal variability is appropriately accounted for.

In this experiment, the GAM specifications employ cyclic spline smoothers for temporal variables (month, hour, and weekday) and smooth spline terms for continuous meteorological covariates. Binary and categorical predictors (including year, holiday, working-day indicators, season, and weather conditions) are incorporated as linear terms through one-hot encoding. This structure allows the model to capture nonlinear temporal and meteorological effects while retaining a transparent additive decomposition for categorical factors. To reproduce the baseline results reported in [38], we interface MATLAB with the Python package `pygam` [39] and follow the preprocessing and random data-splitting strategy described in [38], including cyclic smoothers for temporal variables and Poisson regression [42] to model hourly rental counts as realizations of a count process with intensity governed by additive covariate effects.

Table 3 summarizes the predictive performance of various regression models on the Bike Sharing dataset. Among the implemented approaches, XGBoost achieves the lowest test RMSE ( $37.7 \pm 2.8$ ) confirming the high predictive capacity of black-box ensembles on this dataset. The RFF-temporal model, which applies random Fourier features solely to cyclic temporal covariates (hour, weekday, and month), is able to capture periodic demand patterns but lacks explicit modeling of meteorological or categorical effects. Consequently, its accuracy ( $92.3 \pm 3.5$ ) is comparable to the global GAM ( $88.8 \pm 5.6$ ), while remaining well below the most expressive baselines.

Building on this representation, the proposed mixture-of-GAMs framework significantly improves upon both the global GAM and the RFF-temporal baseline, demonstrating the clear benefit of local adaptivity. Notably, the mixture-of-GAMs model ( $52.5 \pm 2.4$ ) attains a lower test RMSE than the Explainable Boosting Machine ( $57.7 \pm 2.5$ ), establishing it as the most accurate model among the evaluated interpretable and locally adaptive approaches. When compared to the mixture-of-linear-models (MLM) baselines, the mixture-of-GAMs framework not only demonstrates a lower test RMSE but also delivers substantially reduced statistical variability. These results indicate that enriching local mixture components with smooth nonlinear effects provides a systematic advantage

Table 3: Training and test RMSE on the Bike Sharing dataset for a range of regression models, spanning expressive black-box methods, standard interpretable baselines, and locally adaptive mixture-based approaches.

Method	Training RMSE	Test RMSE
MLP	41.3	$47.4 \pm 3.0$
Random Forest	58.3	$72.6 \pm 3.3$
XGBoost	24.8	$37.7 \pm 2.8$
RFF-temporal model	87.5	$92.3 \pm 3.5$
LASSO	141.1	$140.3 \pm 5.0$
MARS	120.9	$122.5 \pm 4.5$
Global GAM	85.9	$88.8 \pm 5.6$
Explainable Boosting Machine	56.4	$57.7 \pm 2.5$
MLM-cell	52.7	$60.9 \pm 7.1$
MLM-EPIC	62.8	$66.7 \pm 6.9$
Mixture of GAMs	48.6	$52.5 \pm 2.4$

over purely linear local models, especially in the presence of heterogeneous temporal structure, such as varying demand patterns across commuting and leisure hours.

As a simple illustration of the interpretability offered by the mixture-of-GAMs model, we examine how the mixture components are activated across temporal contexts. Let  $\gamma_{i,\ell}$  denote the posterior responsibility of mixture component  $\ell$  for data point  $i$  and  $h_i \in \{0, 1, \dots, 23\}$  denote the hour-of-day associated with observation  $i$ . The average posterior responsibility at hour  $h$  for cluster component  $\ell$  is defined as

$$\bar{\gamma}_\ell(h) = \frac{1}{|\mathcal{I}_h|} \sum_{i \in \mathcal{I}_h} \gamma_{i\ell}, \quad \mathcal{I}_h := \{i : h_i = h\}.$$

Figure 13 shows the average posterior responsibilities  $\bar{\gamma}_\ell(h)$  of the eight mixture components, evaluated on the training dataset and plotted as functions of the hour of day. Distinct temporal regimes emerge clearly across the clusters, with several components exhibiting pronounced peaks during morning and evening hours, while others are primarily active during midday or late-evening periods. These patterns are consistent with well-known daily usage behaviors in bike-sharing systems, such as commuting-related activity during peak hours and more flexible or leisure-oriented usage outside these periods.

#### 4.4. Kin40k Dataset

The Kin40k dataset is derived from the forward kinematics of an eight-link robotic arm, requiring the prediction of an end-effector's Euclidean distance from a fixed reference. The target function is characterized by nonlinear trigonometric transformations and strong cross-variable interactions, resulting in a highly non-additive structure. Consequently, globally constrained or strictly additive models face inherent limitations in capturing the full complexity of these configurations.

The numerical results in Table 4 align with these structural characteristics. Within the expressive model class, the MLP and the resampling-based RFF model achieve identical top-tier performance (0.071 test RMSE), significantly outperforming the decision-tree-based ensembles, including XGBoost (0.358) and Random Forest (0.494). This suggests that spectral representations

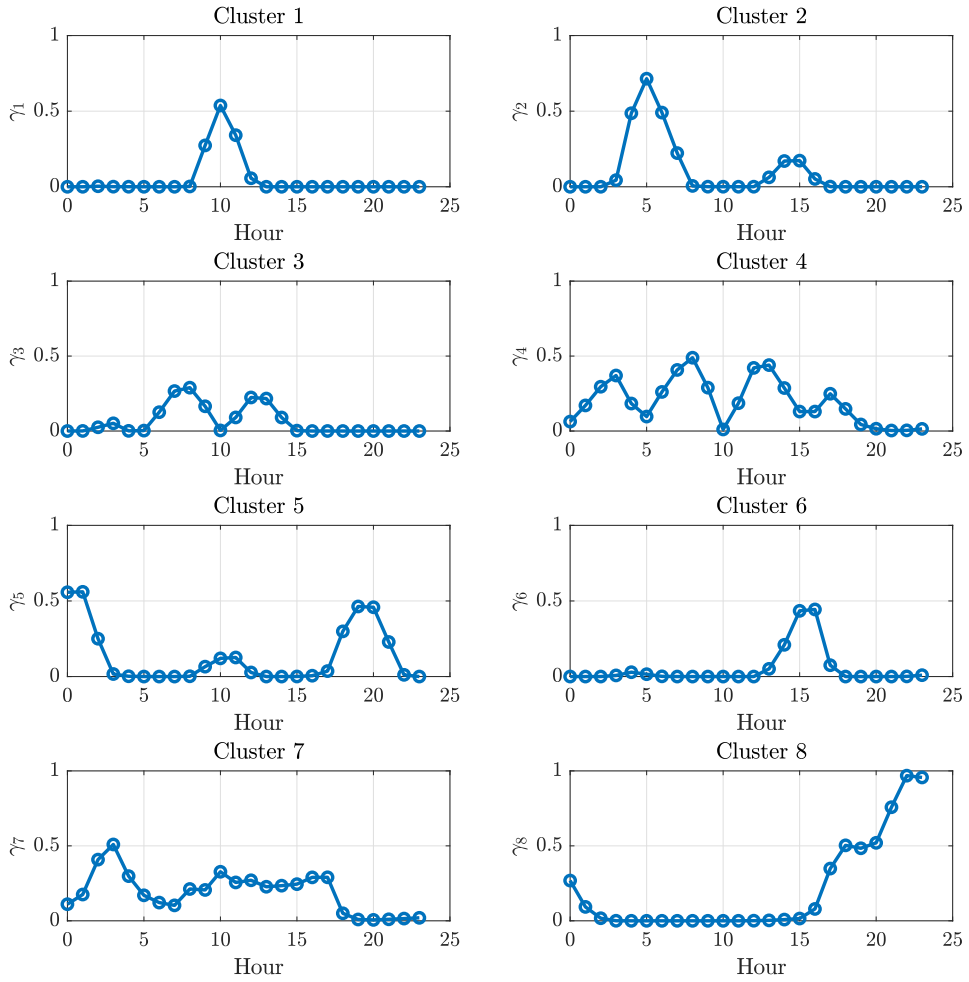


Figure 13: Average posterior responsibilities  $\bar{\gamma}_\ell(h)$  of the eight mixture components as functions of the hour of day, computed over the training dataset.

and deep embeddings are particularly well-suited for capturing the smooth, oscillatory nature of kinematics data.

Among the standard interpretable baselines, the Explainable Boosting Machine ( $0.810 \pm 0.021$ ) provides the strongest global performance, though it remains constrained by its additive assumptions. In contrast, the proposed mixture-of-GAMs framework ( $0.411 \pm 0.012$ ) yields a substantial improvement over all classical interpretable baselines and even outperforms the Random Forest ( $0.494 \pm 0.013$ ). By introducing local adaptivity through RFF-informed clustering, the mixture model successfully alleviates the restrictions of a global additive structure while preserving univariate interpretability within each component. This consistent performance across diverse benchmarks, including the California Housing, Airfoil Self-Noise, and Bike Sharing datasets, further supports the general applicability and stability of the proposed framework.

Table 4: Comparison of root mean square error (RMSE) on the training and test sets of the `kin40k` dataset across seven models: MLP, Random Forest, RFF, LASSO, MARS, global GAM, and locally adaptive mixture of GAMs.

Model	Training RMSE	Test RMSE
MLP	0.059	$0.071 \pm 0.003$
Random Forest	0.388	$0.494 \pm 0.013$
XGBoost	0.206	$0.358 \pm 0.011$
RFF model	0.066	$0.071 \pm 0.004$
LASSO	1.000	$0.971 \pm 0.021$
MARS	0.972	$0.953 \pm 0.022$
Global GAM	0.985	$0.961 \pm 0.021$
Explainable Boosting Machine	0.811	$0.810 \pm 0.021$
Mixture of GAMs	0.400	$0.411 \pm 0.012$

## 5. Conclusion

This work presents a regression framework that combines random Fourier feature representations with cluster-specific generalized additive models to construct locally adaptive predictive models with intrinsic interpretability. The method uses an RFF model to obtain a compact latent representation of the data, from which soft clusters are identified using principal component analysis and a Gaussian mixture model. Within each cluster, a GAM is fitted to capture nonlinear relationships through smooth univariate components, and the overall predictive function is obtained as a weighted combination of these localized models.

Numerical experiments conducted on four benchmark regression datasets, including the California Housing, NASA Airfoil Self-Noise, Bike Sharing, and Kin40k datasets, demonstrate the effectiveness and robustness of the proposed mixture-of-GAMs framework. Across all datasets, the method consistently improves upon global interpretable baselines (LASSO, MARS, and global GAM), highlighting the benefit of combining additive structure with locally adaptive modeling. On the California Housing and Bike Sharing datasets, the mixture of GAMs further attains lower test errors than mixture-of-linear-model (MLM) baselines, indicating that enriching local mixture components with smooth nonlinear effects can provide tangible advantages over purely linear local models. On the Airfoil Self-Noise and Kin40k datasets, the proposed approach achieves performance

comparable to more expressive black-box models, such as Random Forest or multilayer perceptron, while preserving a substantially higher level of interpretability.

Beyond predictive performance, the proposed framework yields interpretable representations that reveal meaningful geometric and structural patterns in the data. In particular, the spatial frequencies learned by the RFF model induce clusters aligned with dominant spatial trends. As demonstrated in Section 4.1.2, restricting the representation to spatial Fourier features uncovers a clear inland-coastal gradient in the California Housing dataset. This example illustrates how spectral information encoded in RFFs can both guide the construction of transparent cluster-wise GAMs and provide insight into large-scale covariate structure, reinforcing the interpretability benefits of the proposed approach.

Taken together, these results suggest that the proposed framework offers a flexible and effective compromise between predictive accuracy and model transparency. The empirical findings indicate that local adaptivity alone already yields meaningful gains over global additive models, while the incorporation of smooth nonlinear effects within each mixture component can further enhance performance in settings with heterogeneous regimes or moderately complex nonlinear structure. At the same time, the moderate but consistent improvements observed across diverse datasets highlight the stability and general viability of the approach, supporting its applicability as a principled alternative to both global explainable models and locally linear mixture-based methods.

Several directions for future research remain. One promising avenue is the extension of the proposed framework to spatio-temporal settings, where random Fourier features can encode both spatial structure and temporal dynamics through joint spectral representations. Such an extension may enable interpretable localized models in applications involving the evolution of physical or environmental systems. Further work could also explore alternative latent representations, multi-scale or hierarchical clustering strategies, and clustering methods that incorporate kernel-induced similarity measures.

## Data Availability

The data used in this study consist of publicly available benchmark datasets, including the California Housing, NASA Airfoil Self-Noise, Bike Sharing, and Kin40k benchmarks, which are cited in the references. The code used to generate the results is available in a public GitHub repository, with the link provided in Appendix A.2.

## CRediT authorship contribution statement

**Xin Huang:** Writing - review & editing, Writing - original draft, Visualization, Software, Methodology, Investigation, Validation, Formal analysis, Conceptualization. **Jia Li:** Writing - review & editing, Methodology, Formal analysis, Conceptualization. **Jun Yu:** Writing - review & editing, Methodology, Formal analysis, Conceptualization, Resources.

## Declaration of Competing Interest

The authors declare that they have no known competing financial interests or personal relationships that could have appeared to influence the work reported in this paper.

## Acknowledgements

This work was supported by Kempe Stiftelserna project JCSMK23-0168. The computations used resources provided by the National Academic Infrastructure for Supercomputing in Sweden (NAIIS) at the PDC Center for High Performance Computing, KTH Royal Institute of Technology, which is partially funded by the Swedish Research Council through grant agreement no. 2022-06725. Jia Li's research is supported by the National Science Foundation under grant CCF-2205004.

## References

- [1] Avron, H., Kapralov, M., Musco, C., Musco, C., Velingker, A., Zandieh, A., *Random Fourier Features for Kernel Ridge Regression: Approximation Bounds and Statistical Guarantees*, Proceedings of the 34th International Conference on Machine Learning, PMLR, 70, 253–262, 2017.
- [2] Bach, F., *On the Equivalence between Kernel Quadrature Rules and Random Feature Expansions*, Journal of Machine Learning Research, 18, 1–38, 2017.
- [3] Bach, F., *Learning Theory from First Principles*, Adaptive Computation and Machine Learning series, The MIT Press, 2024.
- [4] Bishop, C.M., *Pattern Recognition and Machine Learning (Information Science and Statistics)*. Springer-Verlag, 2006.
- [5] de Boor, C., *A Practical Guide to Splines*. Springer-Verlag New York, 1978.
- [6] Breiman, L., *Random Forests*. Machine Learning, 45, 5–32, 2001.
- [7] Brooks, T.F., Pope, D.S., and Marcolini, M.A., *Airfoil Self-Noise and Prediction*. NASA Reference Publication 1218, 1989.
- [8] Caruana, R., Lou, Y., Gehrke, J., Koch, P., Sturm, M., and Elhadad, N., *Intelligible models for healthcare: Predicting pneumonia risk and hospital 30-day readmission*. Proceedings of the 21st ACM SIGKDD International Conference on Knowledge Discovery and Data Mining, 2015.
- [9] Chen, T. and Guestrin, C., *XGBoost: A scalable tree boosting system*. Proceedings of the 22nd ACM SIGKDD International Conference on Knowledge Discovery and Data Mining, 2016.
- [10] Chitta, R., Jin, R., and Jain, A.K. *Efficient Kernel Clustering Using Random Fourier Features*. Proceedings of the 2012 IEEE 12th International Conference on Data Mining, 161–170, 2012.
- [11] Deisenroth, M.P., Faisal, A.A., and Ong, C.S., *Mathematics for Machine Learning*. Cambridge University Press, 2020.
- [12] E, W., *A Mathematical Perspective of Machine Learning*. Proceedings of the International Congress of Mathematicians, 2, 914–954, 2022.
- [13] Fanaee-T, H., Gama, J. *Event Labeling Combining Ensemble Detectors and Background Knowledge*. Progress in Artificial Intelligence, 2, 113–127, 2014.
- [14] Fang, K., Liu, F., Huang, X., and Yang, Y., *End-to-End Kernel Learning via Generative Random Fourier Features*. Pattern Recognition, 134:109057, 2023.

[15] Friedman, J.H., *Multivariate Adaptive Regression Splines*. The Annals of Statistics, 19, 1–67, 1991.

[16] Friedman, J.H. *Greedy Function Approximation: A Gradient Boosting Machine*. The Annals of Statistics, 29, 1189–1232, 2001.

[17] Goodfellow, I., Bengio, Y., and Courville, A. *Deep Learning*. The MIT Press, 2016.

[18] Hastie, T. and Tibshirani, R., *Generalized Additive Models*. Chapman and Hall, New York, 1990.

[19] Hastie, T., Tibshirani, R., and Friedman, J.H., *The Elements of Statistical Learning: Data Mining, Inference, and Prediction*. Springer New York, NY, 2009.

[20] Hodges, J., *Richly Parametrized Linear Models: Additive, Time Series, and Spatial Models Using Random Effects*, Boca Raton: Chapman & Hall/CRC Texts in Statistical Science, 2014.

[21] Huang, X., Kammonen, A., Pandey, A., Sandberg, M., von Schwerin, E., Szepessy, A., and Tempone, R., *Convergence for Adaptive Resampling of Random Fourier Features*. Preprint, <https://doi.org/10.48550/arXiv.2509.03151>, 2025.

[22] Kuhn, M. and Johnson, K., *Applied Predictive Modeling*. Springer New York, NY, 2013.

[23] Murphy, K.P., *Probabilistic Machine Learning: An introduction*. The MIT Press, 2022.

[24] Nguyen, K., Dam, N., Le, T., Nguyen, T.D., and Phung, D., *Clustering Induced Kernel Learning*. Proceedings of Machine Learning Research, 95, 129–144, 2018.

[25] Nori, H., Jenkins, S., Koch, P., and Caruana, R., *InterpretML: A Unified Framework for Machine Learning Interpretability*. Preprint, <https://doi.org/10.48550/arXiv.1909.09223>, 2019.

[26] Pace, R.K. and Barry, R., *Sparse Spatial Autoregressions*. Statistics & Probability Letters, 33(3), 291–297, 1997.

[27] Parzen, E., *On Estimation of a Probability Density Function and Mode*. The Annals of Mathematical Statistics, 33, 1065–1076, 1962.

[28] Pedregosa, F., Varoquaux, G., Gramfort, A., Michel, V., Thirion, B., Grisel, O., Blondel, M., Prettenhofer, P., Weiss, R., Dubourg, V., Vanderplas, J., Passos, A., Cournapeau, D., Brucher, M., Perrot, M., and Duchesnay, E., *Scikit-learn: Machine Learning in Python*. Journal of Machine Learning Research, 12, 2825–2830, 2011.

[29] Rahimi, A. and Recht, B., *Random Features for Large-Scale Kernel Machines*. Advances in Neural Information Processing Systems, 2007.

[30] Rasmussen, C.E. and Williams, C.K.I., *Gaussian Processes for Machine Learning*, The MIT Press, 2006.

[31] Rastgoo, A. and Khajavi, H., *A Novel Study on Forecasting the Airfoil Self-Noise, Using a Hybrid Model Based on the Combination of CatBoost and Arithmetic Optimization Algorithm*. Expert Systems with Applications, 229, 120576, 2023.

- [32] Reddy, T.S., Saketh, V.N.S., and Chandran, M., *Interpretable Graph Neural Networks with Random Fourier Features*. Proceedings of the 39th Conference on Neural Information Processing Systems (NeurIPS 25), 2025.
- [33] Rosenblatt, M., *Remarks on Some Nonparametric Estimates of a Density Function*. The Annals of Mathematical Statistics, 27, 832–837, 1956.
- [34] Rudi, A. and Rosasco, L., *Generalization Properties of Learning with Random Features*, Proceedings of the 31st International Conference on Neural Information Processing Systems (NeurIPS 17), 3218–3228, 2017.
- [35] Rumelhart, D.E., Hinton, G.E., and Williams, R.J., *Learning representations by back-propagating errors*, Nature, 323, 533–536, 1986.
- [36] Schölkopf, B. and Smola, A.J., *Learning with Kernels: Support Vector Machines, Regularization, Optimization, and Beyond*. The MIT Press, 2001.
- [37] Seo, B. and Li, J., *Explainable Machine Learning by SEE-Net: Closing the Gap between Interpretable Models and DNNs*. Scientific Reports, 14, 26302, 2024.
- [38] Seo, B., Lin, L., and Li, J., *Mixture of Linear Models Co-supervised by Deep Neural Networks*. Journal of Computational and Graphical Statistics, 31(4), 1303–1317, 2022.
- [39] Servén, D. and Brummitt, C., *pyGAM: Generalized Additive Models in Python* (software), Version 0.4.1, Zenodo, 2018. doi: 10.5281/zenodo.1208724.
- [40] Tibshirani, R., *Regression Shrinkage and Selection via the Lasso*. Journal of the Royal Statistical Society, Series B, 58, 267–288, 1996.
- [41] Wendland, H., *Scattered Data Approximation*. Cambridge University Press, 2004.
- [42] Wood, S.N., *Generalized Additive Models: An Introduction with R* (2nd ed.). Chapman & Hall/CRC Press, 2017.

## Appendix A. Implementation and Hyperparameter Details

### Appendix A.1. Hyperparameters for the Mixture-of-GAMs Framework

This subsection summarizes the hyperparameter choices used for training the proposed Mixture-of-GAMs framework, including the resampling-based random Fourier feature (RFF) representation, latent-space clustering, and local GAM fitting. These settings were selected a priori and fixed across all reported runs for each dataset. Table A.1 provides a detailed overview of the hyperparameters used for the California Housing, NASA Airfoil Self-Noise, and Bike Sharing datasets.

### Appendix A.2. Baseline Models and Training Configuration

We compare the proposed Mixture-of-GAMs framework with a set of commonly used baseline models for regression, using standard and widely adopted software packages. Random Forest regression was implemented using the `RandomForestRegressor` class from the `scikit-learn` library [28], with 200 trees and square-root feature subsampling at each split. Multivariate adaptive regression splines (MARS) were trained using the `Earth` implementation from the `pyearth` package,

Table A.1: Summary of hyperparameters used for the resampling-based RFF model and the Mixture-of-GAMs framework on the California Housing, Airfoil Self-Noise, Bike Sharing, and Kin40k datasets.

Hyperparameter	Cal. Housing	Airfoil Self-Noise	Bike Sharing	Kin40k
<b>RFF Settings</b>				
Number of Fourier features $K$	4000	2000	2000	4000
Random walk step size $\delta$	0.3	0.1	0.05	0.1
Tikhonov-regularization $\lambda$	0.32	0.06	0.04	0.02
<b>Mixture-of-GAMs Settings</b>				
PCA dimension $d$	2	3	3	6
Number of GMM clusters $L$	8	12	8	18
Number of knots per feature	30	10	10	10
Spline degree	3 (cubic)	3 (cubic)	3 (cubic)	3 (cubic)
Smoothing penalty	2nd-difference	2nd-difference	2nd-difference	2nd-difference
<b>Training Setup</b>				
Training/Test split	80% / 20%	80% / 20%	80% / 20%	90% / 10%
Training dataset size $N$	16512	1202	13903	36000

employing cubic spline basis functions and default knot selection. For the NASA Airfoil Self-Noise dataset, the acoustic frequency variable was log-transformed prior to model fitting.

The multilayer perceptron (MLP) and its associated mixture-of-linear-model variants (MLM-cell and MLM-epic) were trained using the same hyperparameter settings as in [38], ensuring comparability across model classes. Full implementation details, including training scripts and configuration files for all baseline models, are provided in the accompanying public code repository: [https://github.com/XinHuang2022/Mixture\\_of\\_GAMs\\_Informed\\_by\\_Fourier\\_Features](https://github.com/XinHuang2022/Mixture_of_GAMs_Informed_by_Fourier_Features).

## Appendix B. Ablation Study on Clustering Source and Local Model Expressiveness

The ablation variants in Table B.1 are designed to evaluate the distinct contributions of each modeling component within the proposed RFF-informed Mixture-of-GAMs framework. In the variant *Raw data + Local GAM*, clustering is performed directly on the standardized input features, followed by fitting a separate GAM in each resulting cluster. The *PCA data + Local GAM* variant instead applies clustering to a PCA-reduced representation, using the same dimensionality as for the proposed RFF-based embedding reduction. These two comparisons serve as baselines to assess the value of spectral representations for guiding clustering. The *RFF + Local Linear Model* variant retains the RFF-based clustering but replaces local GAMs with  $\ell_2$ -regularized linear models, isolating the contribution of nonlinear additive modeling. Finally, *RFF-based Mixture of GAMs* represents the full proposed method, combining spectral clustering in the RFF-induced feature space with locally adaptive GAMs.

On both the California Housing and Airfoil Self-Noise datasets, the proposed RFF-based Mixture-of-GAMs framework consistently achieves the lowest test RMSE among all variants. Notably, clustering based on raw input features or PCA-reduced representations leads to inferior performance compared to clustering using the RFF-based representation. This highlights that the learned spectral embedding captures structure that is more predictive and better aligned with underlying data regimes. Furthermore, replacing local GAMs with linear models within the same RFF-guided clus-

Table B.1: Ablation study comparing clustering sources and local model expressiveness. All methods use the same number of clusters and identical training protocols. Lower RMSE indicates better performance.

Method	California Housing		Airfoil Self-Noise	
	Train RMSE	Test RMSE	Train RMSE	Test RMSE
Raw data + Local GAM	0.479	$0.538 \pm 0.023$	2.90	$3.35 \pm 0.08$
PCA data + Local GAM	0.507	$0.556 \pm 0.023$	2.50	$3.01 \pm 0.07$
RFF + Local Linear Model	0.629	$0.627 \pm 0.025$	2.61	$2.51 \pm 0.05$
RFF-based Mixture of GAMs	0.442	$0.489 \pm 0.021$	2.01	$2.22 \pm 0.05$

ters substantially degrades accuracy, underscoring the importance of nonlinear additive modeling. These findings confirm that both the spectral representation used for clustering and the expressiveness of the local models are critical to the overall performance of the proposed method.

### Appendix C. Nomenclature and Abbreviations

In this section, we summarize the abbreviations and notation used in this work, as listed in Tables C.1 and C.2.

Table C.1: Abbreviations

Abbreviation	Description
RFF	Random Fourier Features
GAM	Generalized Additive Model
DNN	Deep Neural Network
GMM	Gaussian Mixture Model
MLM	Mixture of Linear Models
PCA	Principal Component Analysis
SVD	Singular Value Decomposition
EM	Expectation-Maximization (algorithm)
LASSO	Least Absolute Shrinkage and Selection Operator
MLP	Multi-Layer Perceptron
MARS	Multivariate Adaptive Regression Splines
RBF	Radial Basis Function

Table C.2: Nomenclature

<b>Vectors, Sets, and Data</b>	
$\{(\mathbf{x}_i, y_i)\}_{i=1}^N$	Training dataset consisting of $N$ input-output pairs
$\mathbf{x} = [x_1, \dots, x_p]^\top \in \mathbb{R}^p$	Input (predictor) vector with $p$ covariates
$y_i \in \mathbb{R}$	Response variable associated with input $\mathbf{x}_i$
$\{\omega_k\}_{k=1}^K$ with $\omega_k \in \mathbb{R}^p$	Set of sampled random Fourier frequencies
$\varsigma(\mathbf{x}) \in \mathbb{C}^K$	Random Fourier feature map evaluated at $\mathbf{x}$
$\beta \in \mathbb{C}^K$	Coefficient vector of the random Fourier feature model
<b>Feature Matrices and PCA Components</b>	
$\mathbf{S} \in \mathbb{R}^{N \times K}$	Random Fourier feature matrix for the training data
$\bar{\mathbf{S}}$	Centered random Fourier feature matrix
$\bar{\mathbf{s}} \in \mathbb{R}^K$	Empirical mean of the random Fourier feature vectors
$\mathbf{U}, \Sigma, \mathbf{V}$	Matrices from the singular value decomposition of $\bar{\mathbf{S}}$
$\mathbf{V}_d \in \mathbb{R}^{d \times K}$	PCA projection matrix retaining the leading $d$ principal components
$\mathbf{Z} \in \mathbb{R}^{N \times d}$	Low-dimensional latent representation of the training data
<b>Functions and Predictive Models</b>	
$m(\mathbf{x})$	Target regression function
$\bar{m}(\mathbf{x})$	Random Fourier feature approximation of $m(\mathbf{x})$
$h(\mathbf{x})$	PCA-reduced latent representation of input $\mathbf{x}$
$\hat{f}^{(\ell)}(\mathbf{x})$	Cluster-specific generalized additive model
$g_j^{(\ell)}(x_j)$	Univariate smooth function for covariate $j$ in cluster $\ell$
$\phi_{j,q}(x_j)$	Spline basis function utilized in the generalized additive model
$\hat{m}(\mathbf{x})$	Aggregated mixture-of-GAMs regression function
<b>Mixture Model Parameters</b>	
$L$	Number of mixture components (clusters)
$\pi_\ell$	Mixing weight of the $\ell$ -th Gaussian component
$\mu_\ell, \Sigma_\ell$	Mean and covariance of the $\ell$ -th Gaussian component
$\gamma_\ell(\mathbf{x})$	Posterior responsibility of cluster $\ell$ for input $\mathbf{x}$
<b>Miscellaneous Symbols</b>	
$\odot$	Hadamard (elementwise) product
$\text{Re}(\cdot)$	Real part of a complex-valued quantity
$\mathcal{N}(\cdot; \mu, \Sigma)$	Multivariate Gaussian distribution with mean $\mu$ and covariance $\Sigma$